

---

# Sensitivity-Aware Amortized Bayesian Inference

---

Lasse Elsemüller  
Heidelberg University

Hans Olischläger  
Heidelberg University

Marvin Schmitt  
University of Stuttgart

Paul-Christian Bürkner  
TU Dortmund University

Ulrich Köthe  
Heidelberg University

Stefan T. Radev  
Rensselaer Polytechnic Institute

## ABSTRACT

Sensitivity analyses reveal the influence of various modeling choices on the outcomes of statistical analyses. While theoretically appealing, they are overwhelmingly inefficient for complex Bayesian models. In this work, we propose sensitivity-aware amortized Bayesian inference (SA-ABI), a multifaceted approach to efficiently integrate sensitivity analyses into simulation-based inference with neural networks. First, we utilize weight sharing to encode the structural similarities between alternative likelihood and prior specifications in the training process with minimal computational overhead. Second, we leverage the rapid inference of neural networks to assess sensitivity to data perturbations and preprocessing steps. In contrast to most other Bayesian approaches, both steps circumvent the costly bottleneck of refitting the model for each choice of likelihood, prior, or data set. Finally, we propose to use deep ensembles to detect sensitivity arising from unreliable approximation (e.g., due to model misspecification). We demonstrate the effectiveness of our method in applied modeling problems, ranging from disease outbreak dynamics and global warming thresholds to human decision-making. Our results support sensitivity-aware inference as a default choice for amortized Bayesian workflows, automatically providing modelers with insights into otherwise hidden dimensions.

## 1 Introduction

Statistical inference aims to extract meaningful insights from empirical data through a series of analytical procedures. Acknowledging that each of these procedures involves a myriad of implicit choices and assumptions, *any single analysis hides an iceberg of uncertainty* (Wagenmakers et al., 2022). We consider *sensitivity analysis* as a formal approach to shed light on this very iceberg of uncertainty.

For instance, global warming forecasts can change depend-

ing on the assumed earth system model. In other words: Climate change analyses can be sensitive to the underlying observation model (i.e., *likelihood*; see **Experiment 2**). Yet, the likelihood is not the only model component that can induce sensitivity. The prior assumptions, the approximation algorithm, and the specifics of the collected data contribute further uncertainty to the results (Bürkner et al., 2022). Classical sensitivity analyses rely on costly model refitting under each configuration and quickly become infeasible for both likelihood-based (e.g., MCMC; Neal, 2011) and simulation-based inference (SBI, Cranmer et al., 2020).

Recently, SBI methods have been accelerated through amortized Bayesian inference (ABI; Vecilla et al., 2022; Gonçalves et al., 2020; Radev et al., 2020), where neural networks learn probabilistic inference tasks and compensate for the training effort with rapid inference on many unseen data sets. As we demonstrate in this paper, this directly enables a large-scale assessment of data sensitivity. However, assessing likelihood, prior, and approximator sensitivity remains extremely challenging in standard ABI applications, which may be costly to train even for a single configuration. To address this gap, we investigate *sensitivity-aware amortized Bayesian inference* (SA-ABI) and demonstrate that it unlocks highly efficient and multifaceted sensitivity analyses in realistic ABI applications (cf. [Figure 1](#)). Our main contributions are:

1. We conceptualize sensitivity via implicit context variables and integrate established methods for sensitivity analysis into amortized Bayesian inference;
2. We investigate a context-aware neural architecture to quantify likelihood and prior sensitivity at inference time with minimal computational overhead and no notable loss of accuracy;
3. We assess approximator sensitivity via deep ensembles and data sensitivity via the near-instant ABI inference;
4. We demonstrate the utility of SA-ABI for quickly assessing sensitivity to more than hundred thousand model configurations in real-world applications.

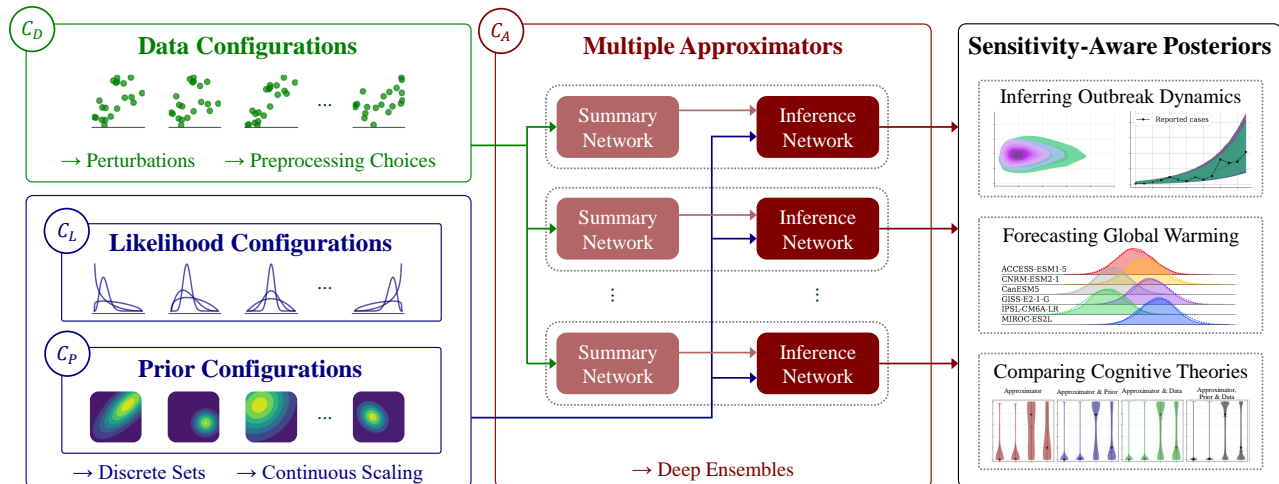


Figure 1: Our proposed approach for sensitivity-aware amortized Bayesian inference (SA-ABI). During training, multiple likelihood, prior, and data configurations are encoded as contexts in a deep ensemble of neural approximators. During inference, our sensitivity-aware method casts model refits as a neural network prediction task which is conditioned on a specific adjustable context  $C$ . This approach unlocks a powerful toolkit of well-established sensitivity analyses for amortized Bayesian inference with negligible computational overhead during inference.

## 2 Background

What follows is a brief overview of Bayesian parameter estimation, model comparison, amortized Bayesian inference, and learnable summary statistics. Readers familiar with these topics can safely jump directly to **Section 3**.

### 2.1 Bayesian Inference

**Bayesian Parameter Estimation** In Bayesian parameter estimation, the key quantity is the *posterior distribution*,

$$p(\theta | \mathbf{x}) = \frac{p(\mathbf{x} | \theta)p(\theta)}{p(\mathbf{x})}, \quad (1)$$

which combines the likelihood  $p(\mathbf{x} | \theta)$  with prior information about parameter distributions  $p(\theta)$ , normalized by the (analytically intractable) marginal likelihood  $p(\mathbf{x})$ .

**Bayesian Model Comparison** In many scientific applications, no single generative model can provide *the* ultimate explanation for a data set  $\mathbf{x}$ . Instead, a set of models  $\mathcal{M} = \{\mathcal{M}_1, \mathcal{M}_2, \dots, \mathcal{M}_J\}$  is plausible. Bayesian model comparison aims to find the “best” model within  $\mathcal{M}$ . In (prior-predictive) Bayesian model comparison, a model’s *marginal likelihood*  $p(\mathbf{x} | \mathcal{M}_j)$  now takes the central role:

$$p(\mathbf{x} | \mathcal{M}_j) = \int p(\mathbf{x} | \theta, \mathcal{M}_j)p(\theta | \mathcal{M}_j) d\theta. \quad (2)$$

Marginalizing the likelihood over the parameter space automatically encodes Occam’s razor through a preference for models with limited prior predictive flexibility

(MacKay, 2003). The *posterior model probabilities* of competing models can be computed as

$$p(\mathcal{M}_j | \mathbf{x}) = \frac{p(\mathbf{x} | \mathcal{M}_j)p(\mathcal{M}_j)}{\sum_{\mathcal{M}} p(\mathbf{x} | \mathcal{M})p(\mathcal{M})}, \quad (3)$$

where  $p(\mathcal{M})$  is the prior distribution over the model space.

### 2.2 Simulation-Based Inference

Both Bayesian parameter estimation and model comparison have traditionally been limited by the ability to efficiently evaluate a model’s likelihood density  $p(\mathbf{x} | \theta)$ . Likelihood-based methods (e.g., MCMC) assume that the distributional family of the likelihood is explicitly known and can be evaluated analytically or numerically for any pair  $(\mathbf{x}, \theta)$ . Differently, simulation-based approaches only require simulations from a simulation program  $G$ ,

$$\mathbf{x} = G(\theta, \xi) \quad \text{with} \quad \xi \sim p(\xi | \theta), \theta \sim p(\theta), \quad (4)$$

with latent program states or “outsourced” noise  $\xi$ . A single execution of such a program corresponds to generating samples from the Bayesian joint model  $(\theta, \mathbf{x}) \sim p(\theta, \mathbf{x})$ , since the execution paths of the simulation program define an *implicit likelihood* (Cranmer et al., 2020)

$$p(\mathbf{x} | \theta) = \int \delta(\mathbf{x} - G(\theta, \xi))p(\xi | \theta) d\xi, \quad (5)$$

where  $\delta$  is the Dirac delta function. However, the above equation (5) is analytically intractable for any simulation program of practical interest, turning simulation-based inference into a computational challenge.

### 2.3 Amortized Bayesian Inference

Amortized Bayesian inference (ABI) leverages simulations from  $G$  to solve Bayesian inference tasks with neural networks in real time after an initial training phase. To achieve this, neural networks learn to encode the relationship between simulated data and model states during training. As a result, costly probabilistic inference is replaced with a neural network prediction task. For parameter estimation, generative neural networks act as conditional neural density approximators of the parameter posterior  $p(\theta | \mathbf{x})$  (Greenberg et al., 2019; Radev et al., 2020). Model comparison, on the other hand, can be framed as a probabilistic classification problem which is addressed with discriminative neural networks to approximate posterior model probability  $p(\mathcal{M} | \mathbf{x})$  (Pudlo et al., 2016; Radev et al., 2021a).

### 2.4 End-to-end Summary Statistics

Common neural density estimators hinge on fixed-length vector-valued inputs – a requirement that is violated by widespread data formats such as sets of *i.i.d.* observations or time series. To this end, previous research explored ways to learn end-to-end summary statistics for flexible adaption to the individual data structure and inference task (Chan et al., 2018; Radev et al., 2020; Wiquvist et al., 2019). In a nutshell, a summary network  $h_\psi$  compresses input data  $\mathbf{x}$  of variable size to a fixed-length vector of learned summary statistics  $h_\psi(\mathbf{x})$  by exploiting probabilistic symmetries in the data (e.g., permutation-invariant networks for exchangeable data; Bloem-Reddy & Teh, 2020). The resulting *embedding* is fed to an inference network  $f_\phi$  that approximates the posterior (e.g., with a conditional normalizing flow). The summary network  $h_\psi$  and the inference network  $f_\phi$  are simultaneously trained end-to-end in order to learn optimal summary statistics for the inference task.

## 3 Methods

The PAD framework (Bürkner et al., 2022) defines a Bayesian model as a combination of the joint Probability distribution  $p(\theta, \mathbf{x} | \mathcal{M})$ , which can be factorized into likelihood  $p(\mathbf{x} | \theta, \mathcal{M})$  and prior  $p(\theta | \mathcal{M})$ , the posterior Approximator, and the observed Data  $\mathbf{x}_{\text{obs}}$ . In the following, we consider potential sources of sensitivity for each component as context variables that implicitly shape inferential results (see Figure 1). In standard workflows, context variables are considered fixed and thus not further specified as explicit conditioning variables (Gelman et al., 2020).

We denote context variables as  $C_L$  (likelihood),  $C_P$  (prior),  $C_A$  (approximator),  $C_D$  (data), and refer to the entirety of context variables as  $C = (C_L, C_P, C_A, C_D)$ . Accordingly, the resulting posteriors can be denoted explicitly as  $p(\theta | \mathbf{x}, C)$  for parameter estimation or  $p(\mathcal{M}_j | \mathbf{x}, C)$  for model comparison. We will refer to the opposite of sensi-

tivity as *robustness*: When an inference procedure is robust, it is not sensitive to changes in context variables.

### 3.1 Extending the Amortization Scope

Before discussing key facets of practical sensitivity analysis, we describe extensions to standard simulation-based training that allow these analyses to be performed *efficiently*. Specifically, we eliminate the necessity of re-training neural approximators for every aspect of sensitivity analysis by incorporating the Training contexts  $C_T = (C_L, C_P)$  into the network’s amortization scope (Radev, 2021). Since we realize  $C_A$  via deep ensembles (see Section 3.3) and  $C_D$  only during inference (see Section 3.4), both do not enter the training objectives of single ensemble members.

For sensitivity-aware parameter estimation (PE), we incorporate the context  $C_T$  into the standard negative log-posterior objective via

$$\mathcal{L}^{\text{PE}}(\phi, \psi; C_T) = \mathbb{E} \left[ -\log q_\phi(\theta | h_\psi(\mathbf{x}), C_T) \right]. \quad (6)$$

The expectation  $\mathbb{E}$  is here taken over a contextualized joint Bayesian model  $p(\theta, \mathbf{x} | C_T)$ , which produces tuples of training parameters and corresponding data  $(\theta, \mathbf{x})$  for the given context  $C_T$ .

Analogously, for sensitivity-aware model comparison (MC), we can target the approximate posterior model probability  $q_\phi(\mathcal{M} | h_\psi(\mathbf{x}), C_T)$  via the cross-entropy

$$\mathcal{L}^{\text{MC}}(\phi, \psi; C_T) = \mathbb{E} \left[ -\sum_{j=1}^J \mathbb{I}_{\mathcal{M}_j} \log q_\phi(\mathcal{M}_j | h_\psi(\mathbf{x}), C_T) \right], \quad (7)$$

where the expectation  $\mathbb{E}$  is taken with respect to a contextualized generative mixture of Bayesian models  $p(\mathcal{M}_j | C_T) p(\mathbf{x} | \mathcal{M}_j, C_T)$  producing tuples of model indices and associated simulated data  $(\mathcal{M}_j, \mathbf{x})$ . The indicator function  $\mathbb{I}_{\mathcal{M}_j}$  denotes a one-hot encoding for the true model index, i.e.,  $\mathbb{I}_{\mathcal{M}_j} = 1$  if  $\mathcal{M}_j$  is the true model.

To achieve the desired amortization over any set of context variables  $C_T$ , we can place a prior distribution over the domains of  $C_T$  and minimize the *context-aware* (CA) loss:

$$\mathcal{L}^{\text{CA}}(\phi, \psi) = \mathbb{E} [\mathcal{L}(\phi, \psi; C_T)], \quad (8)$$

where the (outer) expectation runs over  $p(C_T)$  and  $\mathcal{L}$  can be either  $\mathcal{L}^{\text{PE}}$  or  $\mathcal{L}^{\text{MC}}$ . In practice, we approximate Eq. 8 using standard mini-batch gradient descent over a finite data set  $\mathcal{D} = \{C_T, \theta, \mathbf{x}\}$  for parameter estimation, or  $\mathcal{D} = \{C_T, \mathcal{M}_j, \mathbf{x}\}$  for model comparison.

Our approach seamlessly generalizes to other *strictly proper losses* (Gneiting & Raftery, 2007) which can be used as training objectives for amortized inference (Pacchiardi & Dutta, 2021). For the sake of generality, we can

introduce a function  $S$  that quantifies the fidelity of a conditional distribution  $q_\phi \in \mathcal{Q}$  for predicting a target quantity  $\mathbf{y} \in \mathcal{Y}$  (Gneiting & Raftery, 2007). Thus,  $S : \mathcal{Q} \times \mathcal{Y} \rightarrow \mathbb{R}$  is a function of some  $q_\phi$  and  $\mathbf{y}$  (e.g.,  $\theta$  or  $\mathcal{M}_j$ ) which can easily be written to incorporate arbitrary conditions for  $q_\phi$ , such as summarized data  $h_\psi(\mathbf{x})$  and context  $C_T$ , resulting in  $S(q_\phi(\mathbf{y} | h_\psi(\mathbf{x}), C_T), \mathbf{y})$ . Ideally, we would like to treat the *expected score* as an optimization objective

$$\mathcal{L}(\phi, \psi; C_T) = \mathbb{E}_{p^*(\mathbf{x}, \mathbf{y})} \left[ S(q_\phi(\mathbf{y} | h_\psi(\mathbf{x}), C_T), \mathbf{y}) \right], \quad (9)$$

which for *strictly proper scoring functions*  $S$  would guarantee  $q_\phi(\mathbf{y} | h_\psi(\mathbf{x}), C_T) = p^*(\mathbf{y} | \mathbf{x})$  under perfect convergence (Gneiting & Raftery, 2007; Pacchiardi & Dutta, 2021). However, we usually cannot directly access the analytic expectation over the unknown true data-generating distribution  $p^*(\mathbf{x}, \mathbf{y})$ . Thus, to achieve tractable amortization, we use the model-implied  $p(\mathbf{x}, \mathbf{y} | \mathcal{M})$  as a proxy for  $p^*(\mathbf{x}, \mathbf{y})$  and optimize the above objective in expectation over the simulator (i.e., one or more Bayesian models) outputs.

### 3.2 Likelihood and Prior Sensitivity

Varying likelihood context variables are ubiquitous in simulation-based inference. Structural decisions within the simulator(s) may constitute context variables (e.g., the underlying scientific model, see **Experiment 2**) or exogenous experimental factors, such as design matrices, indicator variables, or time scales. Typical examples for prior context might be as simple as the scales of prior distributions, or as complex as different experts eliciting discrete sets of qualitative (e.g., non-probabilistic) domain knowledge. Moreover, both likelihood and prior can be continuously tempered to strengthen or weaken their influence. For example, power-scaling exponentiates densities with a parameter  $\gamma > 0$ , resulting in  $p(\theta)^\gamma$  for prior power scaling and  $p(\mathbf{y} | \theta)^\gamma$  for likelihood power scaling (Kallioinen et al., 2021).

We make all known pieces of likelihood and prior context explicit by incorporating  $C_L$  and  $C_P$  into the generative model. This enables amortization over these context variables, which drastically increases the generalization space of the trained neural approximator. During inference, the specific set of likelihood and prior can simply be selected by passing the respective  $C_L$  and  $C_P$  configurations. Amortization over the context space leverages structural similarities between context configurations via weight sharing. Compared to separate training, this *minimizes the associated computational cost and is especially beneficial whenever only finite training data is available* (see **Experiment 2**).

Table 1: Comparison of methods for sensitivity analysis in Bayesian inference.

	IJ	IS	ABI	SA-ABI
Can handle intractable likelihoods	✗	✗	✓	✓
Amortized likelihood & prior sensitivity	✓	✓	✗	✓
Amortized data sensitivity	✗	✗	✓	✓

IJ: Infinitesimal Jackknife; IS: Importance Sampling; ABI: Amortized Bayesian Inference; SA-ABI: Sensitivity-Aware ABI (ours).

### 3.3 Approximator Sensitivity

We define approximator sensitivity as the variability of inferential results due to the approximation method employed. To isolate approximator sensitivity in ABI, it seems helpful to (i) distinguish between a *closed world* (i.e., simulations) and *open world* (i.e., empirical data) setting; and (ii) realize an approximator context  $C_A$  via a deep ensemble of  $M$  equally configured and independently trained neural networks  $\{(\phi^{(m)}, \psi^{(m)})\}_{m=1}^M$ .

In the closed-world setting, ground truth values for the approximation targets  $\theta$  or  $\mathcal{M}_j$  are available. Thus, we can readily validate amortized neural approximators on thousands of simulated data sets from the model(s) under consideration. We propose to additionally measure performance variability between the ensemble members to detect approximator sensitivity due to finite training or suboptimal convergence. After validating the approximator in the closed world, we consider the open-world setting, where the true data-generating process is unknown.

As a simulation-based method, ABI assumes that simulations are a faithful representation of a system’s real behavior (Dellaporta et al., 2022). Hence, *simulation gaps*, where atypical data violate this assumption, threaten its credibility (Cannon et al., 2022; Schmitt et al., 2023). In line with current research on instabilities in out-of-distribution (OOD) settings (Fort et al., 2019; Ji et al., 2021; Shamir et al., 2021), we hypothesize that *variability across the  $M$  ensemble members in the open world despite consistent performance in the closed world* indicates a simulation gap. Concretely, we expect a simulation gap to translate into high variability in the predictive distribution of empirical data  $\mathbf{x}_{\text{obs}}$ ,

$$\tilde{q}(\mathbf{y} | \mathbf{x}_{\text{obs}}) = \int q_\phi(\mathbf{y} | h_\psi(\mathbf{x}_{\text{obs}})) p(\phi, \psi | \mathcal{D}) d\phi d\psi, \quad (10)$$

which is approximated by the deep ensemble (Lakshminarayanan et al., 2017) and can be augmented with arbitrary context  $C$ . When we train a deep ensemble with  $M$  members, we clearly need to repeat the training loop  $M$  times. Crucially though, we can simulate a single training set upfront and then re-use the simulated training data for all ensemble members. This not only reduces the stochastic dependence by keeping the training data constant but also

drastically reduces the computational cost in most realistic tasks where simulations are expensive. Finally, our ensemble approach can be easily extended to investigate hyperparameter sensitivity via hyperparameter ensembles (Wenzel et al., 2020) or combine information from all ensemble members for potentially more accurate inference (e.g., via simulation-based stacking, Yao et al., 2023).

### 3.4 Data Sensitivity

Statistical inference relies on finite samples to draw conclusions about populations. As such, any analysis is influenced by the properties of this particular sample. For instance, analysis outcomes might radically change under different preprocessing choices, such as handling extreme or missing data points, even if these choices only affect a small subset (Broderick et al., 2023; Simmons et al., 2011).

There are two straightforward strategies to assess this data sensitivity: (i) To assess a disproportionately large influence of single data points, a context  $C_D$  of alternative data manifestations can be realized via small perturbations of the empirical data set, for instance via bootstrapping or leave-one-out folds; (ii) to analyze the effect of specific preprocessing decisions, we can generate data set variations for all combinations of reasonable decisions, which in turn constitutes  $C_D$ . Both strategies require a large amount of model refits, which is computationally infeasible for MCMC or non-amortized simulation-based approximators. In contrast, ABI methods can amortize across data sets of variable sizes (Radev et al., 2020), enabling rapid inference on a large number of data set variations.

### 3.5 Quantitative Sensitivity

We can easily *quantify* sensitivity via a divergence metric  $\mathbb{D}$  between target probability densities (Kallioinen et al., 2021; Roos et al., 2015): For an acceptable upper bound  $\vartheta$ , a model is robust if

$$\mathbb{D}[p(g(\mathbf{y}) \mid \mathbf{x}, C_1) \parallel p(g(\mathbf{y}) \mid \mathbf{x}, C_2)] < \vartheta, \quad (11)$$

for arbitrary context realizations  $C_1$  and  $C_2$ , where  $g(\mathbf{y})$  is a pushforward variable (e.g., predicted quantities) or a projection of the full target posterior onto a subset  $\mathbf{y}' \subseteq \mathbf{y}$ .

Measures from the family of  $\mathcal{F}$ -divergences offer principled metrics for  $\mathbb{D}$  (Ali & Silvey, 1966; Csiszár, 1964; Liese & Vajda, 2006). In Bayesian model comparison, the model posterior containing the probabilities for each  $\mathcal{M}_j$  follows a discrete categorical distribution. Thus, obtaining  $\mathcal{F}$ -divergences, such as the KL divergence, is straightforward (see **Experiment 3, Figure 5b**). In Bayesian parameter estimation, the posterior is typically not available as a closed-form density but as random draws. Thus, we prefer a probability integral metric, such as the maximum mean discrepancy (MMD; Gretton et al., 2012), which can be efficiently estimated from posterior samples.

### 3.6 Qualitative Sensitivity

Although quantitative sensitivity patterns provide detailed insights, sensitivity analysis is often ultimately interested in *qualitative* robustness, i.e., invariance of analytical conclusions to the context  $C$  (Bürkner et al., 2022; Kallioinen et al., 2021). For instance, an analyst might ask whether two choices of context variables  $C_1$  and  $C_2$  contain a certain parameter value within a specified highest density interval (HDI), or lead to the selection of the same model  $\mathcal{M}_j$  (see **Supplementary Material** for a formal notation).

## 4 Related Work

**Extending the amortization scope** Wu et al. (2020) proposed a variational inference algorithm that amortizes over a family of probabilistic generative models. This approach learns transferable representations and generalizes to unseen distributions within the amortized family. Schröder and Macke (2023) used a similar principle to perform inference on a *set of models* by combining model comparison and parameter estimation into a single mixture generative model. On a related note, Dax et al. (2023) avoid training separate neural approximators for gravitational-wave parameter estimation by conditioning on detector-noise characteristics. Our SA-ABI method integrates ideas from amortization scope extension in a unified framework, enabling amortization over *any* plausible prior, likelihood, and data configurations while also assessing approximator sensitivity.

**Likelihood and prior sensitivity** The posterior distribution clearly depends on the likelihood and prior, and a large body of research has studied the sensitivity to both likelihood and prior (for an overview, see Depaoli et al., 2020; Insua & Ruggeri, 2012). In non-amortized Bayesian inference, several approaches aim to avoid costly model refits by estimating the effects of local likelihood or prior perturbations on a given posterior, for example, via the infinitesimal jackknife (Giordano et al., 2018, 2019) or Pareto-smoothed importance sampling (Kallioinen et al., 2021). However, these approaches require an analytically tractable likelihood function and rather expensive refits to evaluate data sensitivity. SA-ABI, in contrast, allows for a *direct* assessment of posteriors under different  $C_L$  and  $C_P$  contexts while eliminating tractable likelihood restrictions and the computational burden of refits (see **Table 1**).

**Approximator sensitivity** Recent work has employed deep ensembles for posterior estimation (Balabanov et al., 2023; Tiulpin & Blaschko, 2022) or improving the performance of simulation-based inference (Cannon et al., 2022; Modi et al., 2023), but not for quantifying the sensitivity induced by the approximation procedure. Schmitt et al. (2023) developed a method to detect simulation gaps

Table 2: **Experiment 1:** Benchmarking approximation quality and time between standard ABI and SA-ABI (ours) in a limited data setting.

Method	MAE ↓	ECE ↓	PC ↑	Time by # of priors ↓		
	(± SEM)	(± SEM)	(± SEM)	1	3	1 000
ABI	0.73 ± 0.02	0.006 ± 0.002	0.36 ± 0.07	6min	17min	5 802min
SA-ABI	0.71 ± 0.16	0.009 ± 0.002	0.39 ± 0.26	6min	6min	26min

*Note.* SEM = Standard Error of the Mean. MAE = Mean Absolute Error. ECE = Expected Calibration Error. PC = Posterior Contraction. Metrics are averaged over three prior scaling settings  $\gamma \in \{0.5, 1.0, 2.0\}$  with  $N = 1\,000$  held-out data sets each. Total times for training and inference are reported (extrapolated for 1 000 prior sensitivity evaluations).

in amortized Bayesian parameter estimation via out-of-distribution detection. We adopt a similar perspective on simulation gaps but focus on quantifying the resulting sensitivity in both parameter estimation and model comparison based on the variability of ensemble members. Beyond the identification of simulation gaps, SA-ABI has the crucial advantage of directly assessing the *real-life impact* of a simulation gap in terms of unreliable approximation.

**Data sensitivity** The fact that analyses are sensitive to the input sample (i.e., data sensitivity) has wide-ranging implications across the sciences. First, the immoderate influence of single data points is closely related to traditional notions of robustness and simulation-based solutions thereof (Huang et al., 2023; Ward et al., 2022). Framed as a hostile scenario, adversarial attacks intend to exploit data sensitivity (Baruch et al., 2019; Biggio et al., 2012; Goodfellow et al., 2015), and adversarial robustness tries to prevent this (see Glöckler et al., 2023, for an ABI application). Second, the sensitivity to different preprocessing choices is directly linked to the reproducibility crisis in the empirical sciences (OSC, 2015; Wicherts et al., 2016). To render this sensitivity tangible, Steegen et al. (2016) introduced the *multiverse analysis*, which repeats an analysis across all alternatively processed data sets. The concept of a holistic analysis across plausible data configurations has been continually extended but is typically restricted by the computational feasibility of large-scale refits (Hall et al., 2022; Liu et al., 2020) or to specific estimation procedures (Broderick et al., 2023). In summary, our sensitivity-aware method unlocks (i) near-instant analyses of data sensitivity and adversarial susceptibility; and (ii) rapid multiverse analyses across a wide space of data processing decisions.

## 5 Experiments

In the following, we demonstrate the utility of our SA-ABI approach on applied, real-data modeling problems of COVID-19 outbreak dynamics (**Experiment 1**; prior sensitivity), climate modeling (**Experiment 2**; prior and likelihood sensitivity), and human decision-making

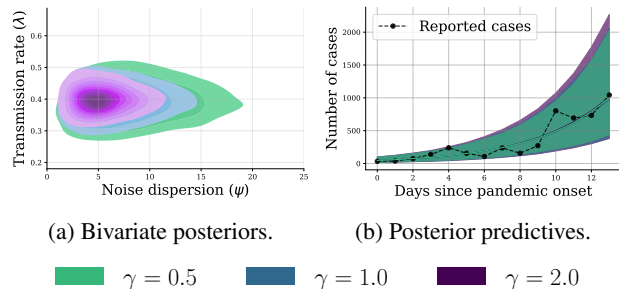


Figure 2: **Experiment 1.** The bivariate posterior (a) of best recoverable parameters  $\lambda$  and  $\psi$  indicates substantial sensitivity in terms of uncertainty reduction for  $\psi$ , but the posterior predictive distribution (b) appears relatively robust (largely overlapping median prediction lines and 90% CIs).

(**Experiment 3**; prior, approximator, and data sensitivity). All implementations use the BayesFlow library for amortized Bayesian workflows (Radev et al., 2023b). Details for all experiments, such as model setup, network training, and additional results are available in **Supplementary Material**.

### 5.1 Experiment 1: COVID-19 Outbreak Dynamics

We set the stage with a straightforward example: Modeling the very early stage of a disease outbreak via a SIR model (Dehning et al., 2020). We demonstrate that obtaining amortized prior sensitivity insights does not compromise the approximation performance compared to standard ABI with the same fixed budget of  $N = 2^{14} = 16\,384$  simulations. The simulation model and network architectures are described in Radev et al. (2021b). During training, we use power-scaling, that is, element-wise exponentiation  $p(\theta)^\gamma$ , to amortize over different priors. We sample the scaling factors in log space,  $\gamma \sim \exp(\mathcal{U}(\log(0.5), \log(2.0)))$ , to ensure equal amounts of widening and shrinking. Thus, the prior context  $C_P$  comprises a vector of scaling powers  $\gamma$ .

We first benchmark our SA-ABI approach against individual ABI instances that are trained solely on the tested setting. Table 2 shows a comparable performance of our SA-ABI approach and individual ABI instances over all three settings  $\gamma \in \{0.5, 1.0, 2.0\}$ , despite spending only a fraction of the simulation budget on the tested settings.

Further, Figure 2 shows the prior sensitivity insights obtained by our SA-ABI approach: The bivariate posteriors for the two parameters with the best recovery (i.e., transmission rate and noise dispersion) unveil that prior sensitivity only affects the noise dispersion (see Figure 2a). Despite prior sensitivity in terms of parameter recoverability, model-based predictive performance is robust to prior scal-

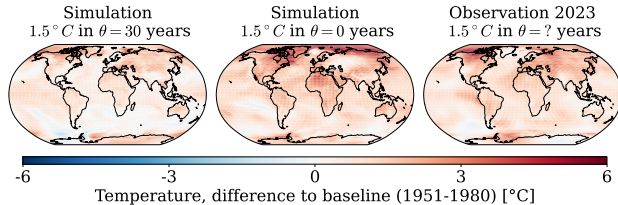


Figure 3: **Experiment 2.** Two examples of simulated observations from the climate model ACCESS-ESM1-5 (SSP-3) with known time-to-threshold (training data) and the current empirical observation that we use for the forecasts.

Table 3: **Experiment 2:** Benchmarking approximation quality and time between standard ABI and SA-ABI (ours) in a limited data setting.

Method	MAE ↓ (± SEM)	ECE ↓ (± SEM)	PC ↑ (± SEM)	Time ↓
ABI	4.24 ± 0.25	0.084 ± 0.016	0.9791 ± 0.0008	313min
<b>SA-ABI</b>	<b>3.80 ± 0.30</b>	<b>0.047 ± 0.008</b>	<b>0.9821 ± 0.0035</b>	<b>67min</b>

*Note.* SEM = Standard Error of the Mean. MAE = Mean Absolute Error. ECE = Expected Calibration Error. PC = Posterior Contraction. Metrics are averaged over test data from all emission scenarios × climate model settings, resulting in 18 combinations with a total of  $N = 2916$  held-out data sets. Total times for training and inference are reported. All networks use the uninformative prior context.

ing (see Figure 2b). The **Supplementary Material** contains additional details and results, including further calibration and recovery diagnostics and MMD hypothesis tests confirming prior sensitivity in the parameter space.

## 5.2 Experiment 2: Climate Trajectory Forecasting

In this experiment, we study whether model-based global warming forecasts are sensitive to the underlying climate model, emission scenario, and prior specification. Climate models estimate the solutions of differential equations for the fluid dynamics and thermodynamics of atmosphere, ocean, ice, and land masses. Since single forecasts can heavily depend on initial conditions, assumed emission scenarios, and the chosen climate model, modern global warming estimates build on a multitude of simulated trajectories (Joshi et al., 2011; Riahi et al., 2017; Zelinka et al., 2020).

However, trajectories simulated from climate models typically start in pre-industrial times, are not explicitly conditioned on any information since 1850, and are only available in a limited number. In their pioneering work, Diffenbaugh and Barnes (2023) combine neural networks trained on simulated trajectories with recent observational data to predict global warming trends and forecast when critical thresholds are reached. Here, we demonstrate the utility of our approach for *efficiently assessing the sensitivity of*

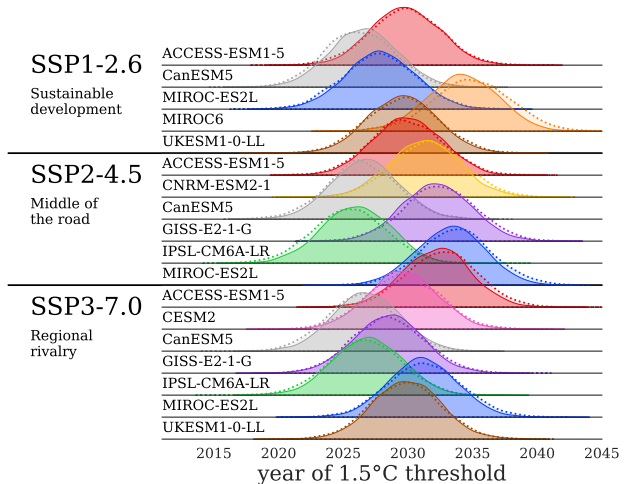
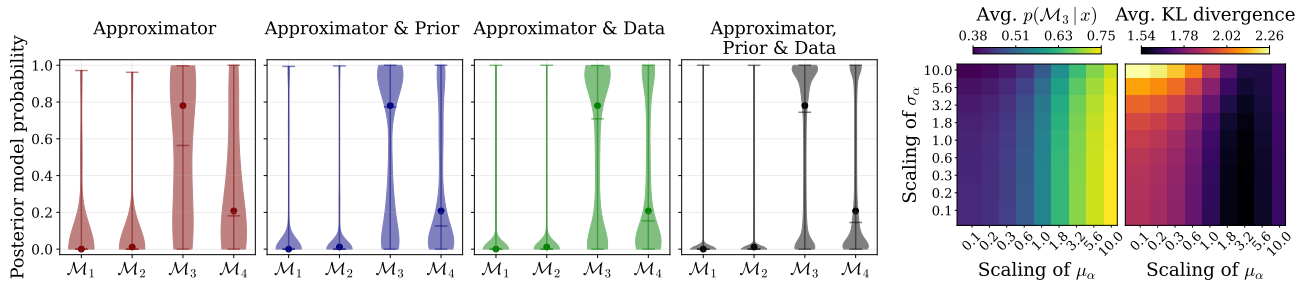


Figure 4: **Experiment 2.** Global warming forecasts are sensitive to the assumed climate model (rows) but not the emission scenario (SSP; groups of rows) or the prior (dotted: weakly informative prior; solid: informative prior).

*model-based predictions* in terms of qualitatively different assumptions regarding the underlying models, emission scenarios, and prior distributions.

Framed as a Bayesian parameter estimation task, we model the time-to-threshold  $\theta$  and explicitly incorporate the climate model and an emission scenario (i.e., SSP1-3) in a likelihood context  $C_L$ . Furthermore, we encode a weakly informative vs. informative prior on  $\theta$  in a prior context  $C_P$  (details in **Supplementary Material**). During training, the neural approximator learns to infer  $\theta$  from simulated observations with the corresponding context. For each training example, we extract the ground truth  $\theta$  from later stages of the simulated trajectory (see Figure 3). At inference time, the network processes an unseen real observation  $x_{\text{obs}}$  from the year 2023 with a context that specifies an emission scenario, a climate model, and a prior configuration. The output is the contextualized approximate posterior  $p(\theta | x_{\text{obs}}, C)$ . We reproduce the results of Diffenbaugh and Barnes (2023) without sacrificing predictive accuracy (see **Supplementary Material**) and reveal sensitivity to the climate model. Further, Table 3 highlights the advantages of our joint training method utilizing information from *all* context configurations via weight sharing, which is especially relevant in the present limited data setting.

Finally, we study the sensitivity of climate forecasts for a real-world question of societal impact: *When will we reach the 1.5°C global warming threshold?* As depicted in Figure 4, the answer to this question is sensitive to the underlying climate model but robust to the assumed emission scenario and informativeness of the prior. This finding is in accordance with Hawkins and Sutton (2009) who argue



(a) Sensitivity to the **approximator**, as well as additional **prior** scaling and **data** perturbations.

(b) Prior sensitivity.

Figure 5: **Experiment 3.** (a) Our sensitivity-aware posterior model probabilities indicate substantial **approximator** sensitivity but robustness to additional **prior** scaling and **data** perturbations. Dots represent the original results by Elsemüller et al. (2023). (b) The posteriors are quantitatively sensitive to power-scaling of the prior location  $\mu_\alpha$ , as indexed by the ensemble-averaged probability for  $\mathcal{M}_3$  (left) as well as the KL divergence between the original results by Elsemüller et al. (2023) vs. scaled model posteriors (right). Notable qualitative sensitivity is present mainly due to different  $\mu_\alpha$  values.

that the delayed effects of emission scenarios are unlikely to show on a short time scale such as the 1.5°C average warming threshold.

### 5.3 Experiment 3: Hierarchical Models of Decision-Making

This experiment extends our method to Bayesian model comparison of complex hierarchical models with analytically intractable likelihoods. The *drift-diffusion model* (DDM) is a popular stochastic model of decision-making widely used in cognitive science and neuroscience (Ratcliff et al., 2016). Elsemüller et al. (2023) recently compared four hierarchical models with ABI to test two proposed improvements of the DDM (referred to as  $\mathcal{M}_1$ ): First, allowing model parameters to vary between experimental trials ( $\mathcal{M}_3$  and  $\mathcal{M}_4$ ) and second, allowing for evidence accumulation “jumps” via an additional parameter  $\alpha$  ( $\mathcal{M}_2$  and  $\mathcal{M}_4$ ).

Elsemüller et al. (2023) found clear evidence for inter-trial variabilities but unclear results concerning the utility of  $\alpha$ . In this experiment, we examine the sensitivity of these results to (i) the prior (via power-scaling the hierarchical prior on  $\alpha$ ), (ii) the approximator (via an ensemble of 20 equally configured neural networks), and (iii) the data (via 100 bootstrap samples). Thus, our comprehensive sensitivity analysis is based on 162 000 posterior model probabilities that are challenging to recover even *once* using existing methods (see **Supplementary Material** for a detailed exposition).

All members of our deep ensemble exhibit near-perfect performance on simulated data, as indexed by average accuracies of .99 and expected calibration errors of .01 (detailed results in **Supplementary Material**, including a benchmark that shows no performance loss by amortizing over  $C_P$ ). Strikingly, Figure 5a reveals highly inconsistent predictions of the ensemble members on the empirical data.

This stark discrepancy implies the presence of a simulation gap. Indeed, contrasting the empirical data with the typical set of model simulations (Morningstar et al., 2021; Nalisnick et al., 2019) flags the empirical data as out-of-distribution for the deep ensemble (see **Supplementary Material**).

Further, Figure 5a shows a comparatively low sensitivity against perturbing the hierarchical prior on  $\alpha$  or the empirical data, with the medians under all perturbations close to the results by Elsemüller et al. (2023). Viewing deep ensemble predictions as approximate Bayesian model averaging (Wilson & Izmailov, 2020), we can conclude that the original results hold, but with substantial OOD uncertainty due to the simulation gap. A closer inspection of prior sensitivity in Figure 5b reveals (i) quantitative sensitivity to wide specifications of the hierarchical location  $\mu_\alpha$ , which increases under narrow specifications of the hierarchical scale  $\sigma_\alpha$ , and (ii) qualitative sensitivity to settings of  $\mu_\alpha$  concerning the model with the highest probability,  $\mathcal{M}_3$ .

## 6 Conclusion

We proposed SA-ABI, an approach for large-scale sensitivity analyses with a keen emphasis on managing uncertainty in critical, high-impact scenarios. By leveraging amortized inference, our method causes minimal computational overhead during inference and can be directly integrated into software toolkits for amortized Bayesian workflows (such as Radev et al., 2023b; Tejero-Cantero et al., 2020). Future work should investigate more efficient approaches to quantify approximator sensitivity, with specific attention to Bayesian neural networks (Izmailov et al., 2021). Additionally, whereas arbitrary data and approximator configurations can be explored at any time, likelihood and prior configurations have to be integrated into the training process. We believe that transfer learning (Bengio et al., 2009; Zhuang et al., 2021) is a promising tool to resolve this con-

straint, unlocking further flexibility on all sensitivity facets.

### Acknowledgements

We thank Noah S. Diffenbaugh and Elizabeth A. Barnes for helping us build upon their pioneering work in Experiment 2. LE was supported by a grant from the Deutsche Forschungsgemeinschaft (DFG, German Research Foundation; GRK 2277) to the research training group Statistical Modeling in Psychology (SMiP) and the Google Cloud Research Credits program with the award GCP19980904. HO was supported by the state of Baden-Württemberg through bwHPC. MS was supported by the Cyber Valley Research Fund (grant number: CyVy-RF-2021-16) and the DFG under Germany's Excellence Strategy EXC-2075 - 390740016 (the Stuttgart Cluster of Excellence SimTech). UK was supported by the Informatics for Life initiative funded by the Klaus Tschira Foundation and the DFG under Germany's Excellence Strategy EXC-2181 - 390900948 (the Heidelberg Cluster of Excellence STRUC-TURES).

### References

- Ali, S. M., & Silvey, S. D. (1966). A general class of coefficients of divergence of one distribution from another. *Journal of the Royal Statistical Society: Series B (Methodological)*, 28(1), 131–142.
- Avecilla, G., Chuong, J. N., Li, F., Sherlock, G., Gresham, D., & Ram, Y. (2022). Neural networks enable efficient and accurate simulation-based inference of evolutionary parameters from adaptation dynamics. *PLoS Biology*, 20(5), e3001633.
- Balabanov, O., Mehlig, B., & Linander, H. (2023). Bayesian posterior approximation with stochastic ensembles. *2023 IEEE/CVF Conference on Computer Vision and Pattern Recognition (CVPR)*.
- Baruch, G., Baruch, M., & Goldberg, Y. (2019). A little is enough: Circumventing defenses for distributed learning. In H. Wallach, H. Larochelle, A. Beygelzimer, F. d'Alché-Buc, E. Fox, & R. Garnett (Eds.), *Advances in neural information processing systems* (Vol. 32). Curran Associates, Inc.
- Bengio, Y., Louradour, J., Collobert, R., & Weston, J. (2009). Curriculum learning. *Proceedings of the 26th annual international conference on machine learning*, 41–48.
- Betancourt, M. (2018). Calibrating model-based inferences and decisions. *arXiv preprint arXiv:1803.08393*.
- Bezanson, J., Edelman, A., Karpinski, S., & Shah, V. B. (2017). Julia: A fresh approach to numerical computing. *SIAM review*, 59(1), 65–98.
- Biggio, B., Nelson, B., & Laskov, P. (2012). Poisoning attacks against support vector machines. *Proceedings of the 29th International Conference on International Conference on Machine Learning*, 1467–1474.
- Bloem-Reddy, B., & Teh, Y. W. (2020). Probabilistic symmetries and invariant neural networks. *J. Mach. Learn. Res.*, 21, 90–1.
- Blumberg, S., Funk, S., & Pulliam, J. R. (2014). Detecting differential transmissibilities that affect the size of self-limited outbreaks. *PLoS pathogens*, 10(10), e1004452.
- Boehm, U., Annis, J., Frank, M. J., Hawkins, G. E., Heathcote, A., Kellen, D., Kryptos, A.-M., Lerche, V., Logan, G. D., Palmeri, T. J., van Ravenzwaaij, D., Servant, M., Singmann, H., Starns, J. J., Voss, A., Wiecki, T. V., Matzke, D., & Wagenmakers, E.-J. (2018). Estimating across-trial variability parameters of the diffusion decision model: Expert advice and recommendations. *Journal of Mathematical Psychology*, 87, 46–75.
- Braumann, A., Krampe, J., Kreiss, J.-P., & Paparoditis, E. (2021). Estimation of the distribution of the individual reproduction number: The case of the covid-19 pandemic. *arXiv preprint arXiv:2101.07919*.
- Broderick, T., Giordano, R., & Meager, R. (2023). An automatic finite-sample robustness metric: When can dropping a little data make a big difference? *arXiv preprint arXiv:2011.14999*.
- Bürkner, P.-C., Scholz, M., & Radev, S. T. (2022). Some models are useful, but how do we know which ones? towards a unified bayesian model taxonomy. *arXiv preprint arXiv:2209.02439*.
- Cannon, P., Ward, D., & Schmon, S. M. (2022). Investigating the impact of model misspecification in neural simulation-based inference. *arXiv preprint arXiv:2209.01845*.
- Chan, J., Perrone, V., Spence, J., Jenkins, P., Mathieson, S., & Song, Y. (2018). A likelihood-free inference framework for population genetic data using exchangeable neural networks. *Advances in neural information processing systems*, 31.
- Cranmer, K., Brehmer, J., & Louppe, G. (2020). The frontier of simulation-based inference. *Proceedings of the National Academy of Sciences*, 117(48), 30055–30062.
- Csiszár, I. (1964). Eine informationstheoretische ungleichung und ihre anwendung auf beweis der ergodizitaet von markoffschen ketten. *Magyer Tud. Akad. Mat. Kutato Int. Koezl.*, 8, 85–108.
- Dax, M., Green, S. R., Gair, J., Pürerer, M., Wildberger, J., Macke, J. H., Buonanno, A., & Schölkopf, B. (2023). Neural importance sampling for rapid and reliable gravitational-wave inference. *Physical Review Letters*, 130(17), 171403.
- Dehning, J., Zierenberg, J., Spitzner, F. P., Wibral, M., Neto, J. P., Wilczek, M., & Priesemann, V. (2020).

- Inferring change points in the spread of covid-19 reveals the effectiveness of interventions. *Science*, 369(6500), eabb9789.
- Dellaporta, C., Knoblauch, J., Damoulas, T., & Briol, F.-X. (2022). Robust bayesian inference for simulator-based models via the mmd posterior bootstrap. *International Conference on Artificial Intelligence and Statistics*, 943–970.
- Depaoli, S., Winter, S. D., & Visser, M. (2020). The importance of prior sensitivity analysis in bayesian statistics: Demonstrations using an interactive shiny app. *Frontiers in Psychology*, 11.
- Diffenbaugh, N. S., & Barnes, E. A. (2023). Data-driven predictions of the time remaining until critical global warming thresholds are reached. *Proceedings of the National Academy of Sciences*, 120(6), e2207183120.
- Els Müller, L., Schnuerch, M., Bürkner, P.-C., & Radev, S. T. (2023). A deep learning method for comparing bayesian hierarchical models. *arXiv preprint arXiv:2301.11873*.
- Fort, S., Hu, H., & Lakshminarayanan, B. (2019). Deep ensembles: A loss landscape perspective. *arXiv preprint arXiv:1912.02757*.
- Gelman, A., Hwang, J., & Vehtari, A. (2014). Understanding predictive information criteria for bayesian models. *Statistics and computing*, 24(6), 997–1016.
- Gelman, A., Vehtari, A., Simpson, D., Margossian, C. C., Carpenter, B., Yao, Y., Kennedy, L., Gabry, J., Bürkner, P.-C., & Modrák, M. (2020). Bayesian workflow. *arXiv preprint arXiv:2011.01808*.
- Giordano, R., Broderick, T., & Jordan, M. I. (2018). Covariances, robustness and variational bayes. *Journal of Machine Learning Research*, 19(1), 1981–2029.
- Giordano, R., Stephenson, W., Liu, R., Jordan, M., & Broderick, T. (2019). A swiss army infinitesimal jack-knife. In K. Chaudhuri & M. Sugiyama (Eds.), *Proceedings of the twenty-second international conference on artificial intelligence and statistics* (pp. 1139–1147, Vol. 89). PMLR.
- Glöckler, M., Deistler, M., & Macke, J. H. (2023). Adversarial robustness of amortized bayesian inference. *arXiv preprint arXiv:2305.14984*.
- Gneiting, T., & Raftery, A. E. (2007). Strictly proper scoring rules, prediction, and estimation. *Journal of the American statistical Association*, 102(477), 359–378.
- Gonçalves, P. J., Lueckmann, J.-M., Deistler, M., Nonnenmacher, M., Öcal, K., Bassetto, G., Chintaluri, C., Podlaski, W. F., Haddad, S. A., Vogels, T. P., et al. (2020). Training deep neural density estimators to identify mechanistic models of neural dynamics. *Elife*, 9, e56261.
- Goodfellow, I., Shlens, J., & Szegedy, C. (2015). Explaining and harnessing adversarial examples. *International Conference on Learning Representations*.
- Greenberg, D., Nonnenmacher, M., & Macke, J. (2019). Automatic posterior transformation for likelihood-free inference. *International Conference on Machine Learning*, 2404–2414.
- Gretton, A., Borgwardt, K., Rasch, M., Schölkopf, B., & Smola, A. (2012). A kernel two-sample test. *The Journal of Machine Learning Research*, 13, 723–773.
- Hall, B. D., Liu, Y., Jansen, Y., Dragicevic, P., Chevalier, F., & Kay, M. (2022). A survey of tasks and visualizations in multiverse analysis reports. *Computer Graphics Forum*, 41(1), 402–426.
- Hawkins, E., & Sutton, R. (2009). The Potential to Narrow Uncertainty in Regional Climate Predictions. *Bulletin of the American Meteorological Society*, 90(8), 1095–1108.
- Huang, D., Bharti, A., Souza, A., Acerbi, L., & Kaski, S. (2023). Learning robust statistics for simulation-based inference under model misspecification. *arXiv preprint arXiv:2305.15871*.
- Insua, D. R., & Ruggeri, F. (2012). *Robust bayesian analysis*. Springer Science & Business Media.
- Izmailov, P., Vikram, S., Hoffman, M. D., & Wilson, A. G. G. (2021). What are bayesian neural network posteriors really like? *International conference on machine learning*, 4629–4640.
- Ji, X., Pascanu, R., Hjelm, R. D., Vedaldi, A., Lakshminarayanan, B., & Bengio, Y. (2021). Predicting unreliable predictions by shattering a neural network.
- Joshi, M., Hawkins, E., Sutton, R., Lowe, J., & Frame, D. (2011). Projections of when temperature change will exceed 2 °C above pre-industrial levels. *Nature Climate Change*, 1(8), 407–412.
- Kallioinen, N., Paananen, T., Bürkner, P.-C., & Vehtari, A. (2021). Detecting and diagnosing prior and likelihood sensitivity with power-scaling. *arXiv preprint arXiv:2107.14054*.
- Kingma, D. P., & Ba, J. L. (2015). Adam: A method for stochastic optimization. *3rd International Conference on Learning Representations*, 1–15.
- Lakshminarayanan, B., Pritzel, A., & Blundell, C. (2017). Simple and scalable predictive uncertainty estimation using deep ensembles. *Advances in neural information processing systems*, 30.
- Lee, J.-Y., Marotzke, J., Bala, G., Cao, L., Corti, S., Dunne, J. P., Engelbrecht, F., Fischer, E., Fyfe, J. C., Jones, C., et al. (2021). Future global climate: Scenario-based projections and near-term information. In *Climate change 2021: The physical science basis. contribution of working group I to the sixth assessment report of the intergovernmental*

- tal panel on climate change* (pp. 553–672). Cambridge University Press.
- Lerche, V., & Voss, A. (2016). Model complexity in diffusion modeling: Benefits of making the model more parsimonious. *Frontiers in Psychology*, 7(1324), 1–14.
- Liese, F., & Vajda, I. (2006). On divergences and informations in statistics and information theory. *IEEE Transactions on Information Theory*, 52(10), 4394–4412.
- Liu, Y., Althoff, T., & Heer, J. (2020). Paths explored, paths omitted, paths obscured: Decision points & selective reporting in end-to-end data analysis. *Proceedings of the 2020 CHI Conference on Human Factors in Computing Systems*.
- MacKay, D. (2003). *Information theory, inference and learning algorithms*. Cambridge University Press.
- Modi, C., Pandey, S., Ho, M., Hahn, C., Blancard, B., & Wandelt, B. (2023). Sensitivity analysis of simulation-based inference for galaxy clustering. *arXiv preprint arXiv:2309.15071*.
- Morningstar, W., Ham, C., Gallagher, A., Lakshminarayanan, B., Alemi, A., & Dillon, J. (2021). Density of states estimation for out of distribution detection. *International Conference on Artificial Intelligence and Statistics*, 3232–3240.
- Naeini, M. P., Cooper, G., & Hauskrecht, M. (2015). Obtaining well calibrated probabilities using bayesian binning. *Proceedings of the Twenty-Ninth AAAI Conference on Artificial Intelligence*, 2901–2907.
- Nalisnick, E., Matsukawa, A., Teh, Y. W., & Lakshminarayanan, B. (2019). Detecting out-of-distribution inputs to deep generative models using typicality. *arXiv preprint arXiv:1906.02994*.
- Neal, R. M. (2011). Mcmc using hamiltonian dynamics. In S. Brooks, A. Gelman, G. Jones, & X.-L. Meng (Eds.), *Handbook of markov chain monte carlo*. Chapman; Hall/CRC.
- OSC. (2015). Estimating the reproducibility of psychological science [Published by the Open Science Collaboration (OSC)]. *Science*, 349(6251).
- Pacchiardi, L., & Dutta, R. (2021). Generalized bayesian likelihood-free inference using scoring rules estimators. *arXiv preprint arXiv:2104.03889*.
- Pudlo, P., Marin, J.-M., Estoup, A., Cornuet, J.-M., Gautier, M., & Robert, C. P. (2016). Reliable abc model choice via random forests. *Bioinformatics*, 32(6), 859–866.
- Radev, S. (2021). *Deep learning architectures for amortized bayesian inference in cognitive modeling* [Doctoral dissertation, Heidelberg University].
- Radev, S. T., D’Alessandro, M., Mertens, U. K., Voss, A., Köthe, U., & Bürkner, P.-C. (2021a). Amortized bayesian model comparison with evidential deep learning. *IEEE Transactions on Neural Networks and Learning Systems*.
- Radev, S. T., Graw, F., Chen, S., Mutters, N. T., Eichel, V. M., Bärnighausen, T., & Köthe, U. (2021b). OutbreakFlow: Model-based Bayesian inference of disease outbreak dynamics with invertible neural networks and its application to the COVID-19 pandemics in germany. *PLoS computational biology*.
- Radev, S. T., Mertens, U. K., Voss, A., Ardizzone, L., & Köthe, U. (2020). Bayesflow: Learning complex stochastic models with invertible neural networks. *IEEE transactions on neural networks and learning systems*.
- Radev, S. T., Schmitt, M., Pratz, V., Picchini, U., Köthe, U., & Bürkner, P.-C. (2023a). JANA: Jointly Amortized Neural Approximation of Complex Bayesian Models. In R. J. Evans & I. Shpitser (Eds.), *Proceedings of the 39th conference on uncertainty in artificial intelligence* (pp. 1695–1706, Vol. 216). PMLR.
- Radev, S. T., Schmitt, M., Schumacher, L., Else Müller, L., Pratz, V., Schälte, Y., Köthe, U., & Bürkner, P.-C. (2023b). Bayesflow: Amortized bayesian workflows with neural networks. *arXiv preprint arXiv:2306.16015*.
- Ratcliff, R. (1978). A theory of memory retrieval. *Psychological review*, 85(2), 59.
- Ratcliff, R., Smith, P. L., Brown, S. D., & McKoon, G. (2016). Diffusion decision model: Current issues and history. *Trends in cognitive sciences*, 20(4), 260–281.
- Riahi, K., Van Vuuren, D. P., Kriegler, E., Edmonds, J., O’Neill, B. C., Fujimori, S., Bauer, N., Calvin, K., Dellink, R., Fricko, O., Lutz, W., Popp, A., Cuaresma, J. C., Kc, S., Leimbach, M., Jiang, L., Kram, T., Rao, S., Emmerling, J., . . . Tavoni, M. (2017). The Shared Socioeconomic Pathways and their energy, land use, and greenhouse gas emissions implications: An overview. *Global Environmental Change*, 42, 153–168.
- Roos, M., Martins, T. G., Held, L., & Rue, H. (2015). Sensitivity analysis for bayesian hierarchical models. *Bayesian Analysis*, 10(2), 321–349.
- Schmitt, M., Bürkner, P.-C., & Köthe. (2023). Detecting model misspecification in amortized bayesian inference with neural networks. *Proceedings of the German Conference on Pattern Recognition (GCPR)*.
- Schröder, C., & Macke, J. H. (2023). Simultaneous identification of models and parameters of scientific simulators. *arXiv preprint arXiv:2305.15174*.
- Shamir, A., Melamed, O., & BenShmuel, O. (2021). The dimpled manifold model of adversarial

- examples in machine learning. *arXiv preprint arXiv:2106.10151*.
- Simmons, J. P., Nelson, L. D., & Simonsohn, U. (2011). False-positive psychology. *Psychological Science*, 22(11), 1359–1366.
- Steege, S., Tuerlinckx, F., Gelman, A., & Vanpaemel, W. (2016). Increasing transparency through a multi-verse analysis. *Perspectives on Psychological Science*, 11(5), 702–712.
- Talts, S., Betancourt, M., Simpson, D., Vehtari, A., & Gelman, A. (2018). Validating bayesian inference algorithms with simulation-based calibration. *arXiv preprint arXiv:1804.06788*.
- Tejero-Cantero, A., Boelts, J., Deistler, M., Lueckmann, J.-M., Durkan, C., Gonçalves, P. J., Greenberg, D. S., & Macke, J. H. (2020). Sbi—a toolkit for simulation-based inference. *arXiv preprint arXiv:2007.09114*.
- Tiulpin, A., & Blaschko, M. B. (2022). Greedy bayesian posterior approximation with deep ensembles. *Transactions on Machine Learning Research*.
- Vehtari, A., Gelman, A., & Gabry, J. (2017). Practical bayesian model evaluation using leave-one-out cross-validation and waic. *Statistics and computing*, 27, 1413–1432.
- Voss, A., Lerche, V., Mertens, U., & Voss, J. (2019). Sequential sampling models with variable boundaries and non-normal noise: A comparison of six models. *Psychonomic bulletin & review*, 26(3), 813–832.
- Wagenmakers, E.-J., Sarafoglou, A., & Aczel, B. (2022). One statistical analysis must not rule them all. *Nature*, 605(7910), 423–425.
- Ward, D., Cannon, P., Beaumont, M., Fasiolo, M., & Schmon, S. (2022). Robust neural posterior estimation and statistical model criticism. *Advances in Neural Information Processing Systems*, 35, 33845–33859.
- Wenzel, F., Snoek, J., Tran, D., & Jenatton, R. (2020). Hyperparameter ensembles for robustness and uncertainty quantification. *Advances in Neural Information Processing Systems*, 33, 6514–6527.
- Wicherts, J. M., Veldkamp, C. L. S., Augusteijn, H. E. M., Bakker, M., van Aert, R. C. M., & van Assen, M. A. L. M. (2016). Degrees of freedom in planning, running, analyzing, and reporting psychological studies: A checklist to avoid p-hacking. *Frontiers in Psychology*, 7.
- Wieschen, E. M., Voss, A., & Radev, S. (2020). Jumping to conclusion? a lévy flight model of decision making. *The Quantitative Methods for Psychology*, 16(2), 120–132.
- Wilson, A. G., & Izmailov, P. (2020). Bayesian deep learning and a probabilistic perspective of generalization. *Advances in neural information processing systems*, 33, 4697–4708.
- Wiqvist, S., Mattei, P.-A., Picchini, U., & Frellesen, J. (2019). Partially exchangeable networks and architectures for learning summary statistics in approximate bayesian computation. *International Conference on Machine Learning*, 6798–6807.
- Wu, M., Choi, K., Goodman, N., & Ermon, S. (2020). Meta-amortized variational inference and learning. *Proceedings of the AAAI Conference on Artificial Intelligence*, 34(04), 6404–6412.
- Yao, Y., Blancard, B. R.-S., & Domke, J. (2023). Simulation based stacking.
- Zaheer, M., Kottur, S., Ravanbakhsh, S., Póczos, B., Salakhutdinov, R. R., & Smola, A. J. (2017). Deep sets. *Advances in neural information processing systems*, 30.
- Zelinka, M. D., Myers, T. A., McCoy, D. T., Po-Chedley, S., Caldwell, P. M., Ceppi, P., Klein, S. A., & Taylor, K. E. (2020). Causes of Higher Climate Sensitivity in CMIP6 Models. *Geophysical Research Letters*, 47(1), e2019GL085782.
- Zhuang, F., Qi, Z., Duan, K., Xi, D., Zhu, Y., Zhu, H., Xiong, H., & He, Q. (2021). A comprehensive survey on transfer learning. *Proceedings of the IEEE*, 109(1), 43–76.

---

## Supplementary Material

---

### A Frequently Asked Questions (FAQ)

#### Q: How can I reproduce the results?

Code for reproducing all results from this paper is freely available at [removed until publication].

#### Q: Can I apply your sensitivity-aware approach to posterior predictive model comparison as well?

Yes! In this work, we focus on prior predictive model comparison, but our ideas directly apply to posterior predictive metrics (Gelman et al., 2014), such as leave-one-out cross-validation (Vehtari et al., 2017). We recommend the joint usage of a posterior and a likelihood network as proposed in Radev et al. (2023a) to achieve amortization in this application.

#### Q: Are there limits to the distributional shapes that can be explored in $C_L$ and $C_P$ ?

The only requirement for distributions in the likelihood and prior context is being able to simulate data from the resulting model. Besides that, SA-ABI gives modelers full flexibility in specifying any theoretically meaningful alternative formulations without concerns about analytically tractable likelihoods, unlike MCMC methods.

#### Q: How exactly did you encode the context variables $C_L$ and $C_P$ in a suitable format for the neural network in your experiments?

In **Experiment 1** and **Experiment 3**, each prior distribution over a parameter is continuously tempered by power-scaling. Consequently,  $C_P$  is encoded by a vector holding the scaling factors for each prior component. In **Experiment 2**, both  $C_L$  and  $C_P$  consist of discrete choices and are therefore passed to the neural network in one-hot-encoded vectors.

### B Methods: Additional Details

#### B.1 Hypothesis Testing for Quantitative Sensitivity

We can employ a sampling-based (frequentist) hypothesis test to determine the probability of observed  $\mathbb{D}(\cdot || \cdot)$  estimates (hitherto referred to as  $\widehat{\mathbb{D}}$ ) under the null hypothesis of zero difference between  $p(\boldsymbol{\theta} | \boldsymbol{x}, C_i)$  and  $p(\boldsymbol{\theta} | \boldsymbol{x}, C_j)$ . For this, we can construct an approximate sampling distribution of  $\widehat{\mathbb{D}}$  under the null hypothesis via bootstrap or permutation tests based on multiple draws from  $p(\boldsymbol{\theta} | \boldsymbol{x}, C_i)$ . Based on the approximate sampling distribution, we can then obtain a critical  $\widehat{\mathbb{D}}$  value for a fixed Type I error probability  $\delta$  and compare it to the observed one. The power of such a test will generally be high when having access to many draws from  $p(\boldsymbol{\theta} | \boldsymbol{x}, C_i)$  and  $p(\boldsymbol{\theta} | \boldsymbol{x}, C_j)$ , a requirement that is easily met in the context of ABI.

#### B.2 Formal Notation for Qualitative Sensitivity

Making decisions based on a posterior distribution can be formalized via a decision function  $L : \mathcal{P} \rightarrow \mathcal{A}$  which maps distributions  $p \in \mathcal{P}$  (or their approximations) to possible qualitative conclusions or actions for a given problem  $a \in \mathcal{A}$ . Formally, qualitative robustness is expressed with the indicator function

$$R(C_1, C_2) = \begin{cases} 1 & \text{if } L(p(\boldsymbol{\theta} | \boldsymbol{x}, C_i)) = L(p(\boldsymbol{\theta} | \boldsymbol{x}, C_j)) \\ 0 & \text{otherwise} \end{cases} \quad (12)$$

which yields 1 if a conclusion is invariant to the choice of arbitrary context realizations  $C_i$  or  $C_j$ , and 0 otherwise. Note that our definition trivially generalizes to more than two choices of context variables  $C$ .

## C Experiments: Implementation Details and Additional Results

### C.1 Benchmarking Metrics

For the benchmarks conducted in **Experiment 1** and **Experiment 2**, we measure three complementary performance metrics on  $J$  unseen test data sets  $\{\mathcal{D}_o^{(j)}\}_{j=1}^J$  with known ground-truth parameters  $\{\theta_*^{(j)}\}_{j=1}^J$ . For each data set  $\mathcal{D}_o^{(j)}$ , we obtain a set  $\{\theta_s^{(j)}\}_{s=1}^S$  of  $S$  posterior draws from the neural approximator  $q_\phi(\theta \mid \mathcal{D}_o^{(j)})$ . We summarize each metric into a single measure across all test data sets and parameters for a given neural approximator and test setting (e.g.,  $\gamma = 0.5$  in **Experiment 1**).

We use the *Mean Absolute Error* (MAE) to measure the overall error between posterior draws  $\theta_s^{(j)}$  and ground-truth parameters  $\theta_*^{(j)}$ :

$$\text{MAE} = \frac{1}{J} \sum_{j=1}^J \left| \frac{1}{S} \sum_{s=1}^S (\theta_s^{(j)} - \theta_*^{(j)}) \right|. \quad (13)$$

Further, we assess uncertainty calibration via the *Expected Calibration Error* (ECE). In Bayesian parameter estimation, all uncertainty regions  $U_q(\theta \mid \mathcal{D})$  of the true posterior  $p(\theta \mid \mathcal{D})$  are by definition well-calibrated for any quantile  $q \in (0, 1)$  (Bürkner et al., 2022), such that:

$$q = \iint \mathbf{I}[\theta_* \in U_q(\theta \mid \mathcal{D})] p(\mathcal{D} \mid \theta_*) p(\theta_*) d\theta_* d\mathcal{D}, \quad (14)$$

with  $\mathbf{I}[\cdot]$  denoting the indicator function. Simulation-based calibration (SBC; Talts et al., 2018) measures miscalibration via deviations from this equality. We estimate the ECE via the median SBC error of 20 linearly spaced credible intervals with quantiles of  $q \in [0.5\%, 99.5\%]$ .<sup>1</sup> Lastly, we measure Bayesian information gain via the median *Posterior Contraction* (PC) across data sets, defined as  $1 - \text{Var}(\text{Posterior})/\text{Var}(\text{Prior})$  (Betancourt, 2018).

### C.2 Experiment 1: COVID-19 Outbreak Dynamics

**Model Setup:** We consider a simple SIR model where individuals are either susceptible,  $S$ , infected,  $I$ , or recovered,  $R$ . Both infection and recovery are modeled with a constant transmission rate  $\lambda$  and recovery rate  $\mu$ , respectively. The model is described by a system of ordinary differential equations (ODEs),

$$\frac{dS}{dt} = -\lambda \left( \frac{SI}{N} \right), \quad (15)$$

$$\frac{dI}{dt} = \lambda \left( \frac{SI}{N} \right) - \mu I, \quad (16)$$

$$\frac{dR}{dt} = \mu I, \quad (17)$$

with  $N = S + I + R$  denoting the total population size. In addition to the ODE parameters  $\lambda$  and  $\mu$ , our model includes a reporting delay parameter  $D$  and a noise dispersion parameter  $\psi$ , which jointly influence the (noisy) number of reported infected individuals via

$$I_t^{(obs)} \sim \text{NegBinomial}(I_{t-D}^{(new)}, \psi), \quad (18)$$

with  $I^{(new)} = \lambda(S_t I_t / N)$ . The negative binomial distribution allows for modeling dispersion, i.e., variation of the variability independent of the mean, which is considered likely for early phases of the COVID-19 pandemic (Blumberg et al., 2014; Braumann et al., 2021). For our implementation, we transform the parameterization in Equation 18 with mean  $I_{t-D}^{(new)}$  and dispersion  $\psi$  to the `numpy` library’s implementation of the negative binomial distribution with number of successes  $n$  and probability of success  $p$ :

$$n = \psi \quad (19)$$

$$\sigma = \frac{I_{t-D}^{(new)} + 1}{\psi (I_{t-D}^{(new)})^2} \quad (20)$$

$$p = \frac{\sigma - I_{t-D}^{(new)}}{\sigma}. \quad (21)$$

<sup>1</sup>In **Experiment 3**, we use the ECE formulation by Naeini et al. (2015) for probabilistic classification.

The fifth estimated model parameter is the initial number of infected individuals  $I_0$ .

We use the same prior specification as Radev et al. (2021b), which is displayed in Table 4 along with the respective power-scaling scheme. Figure 6 shows the behavior of the prior predictive distributions under different power-scaling values  $\gamma$ .

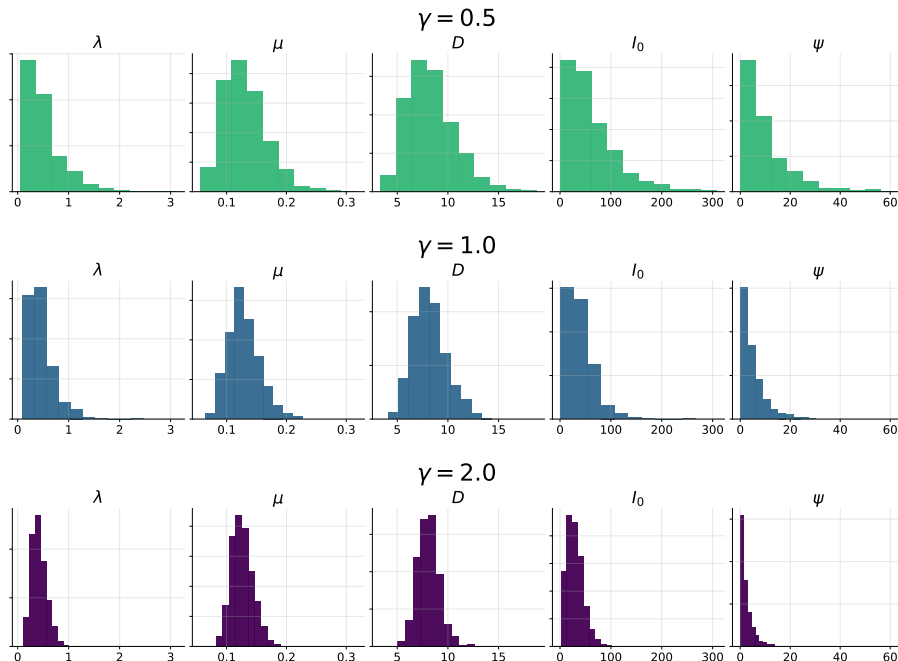


Figure 6: **Experiment 1.** Prior predictive distributions under different scaling parameters  $\gamma$ .

Table 4: **Experiment 1.** Power-scaled prior distributions for all parameters.

Parameter	Symbol	Power-scaled prior distribution
Transmission rate	$\lambda$	$\text{LogNormal}(\log(0.4), 0.5/\sqrt{\gamma_1})$
Recovery rate of infected individuals	$\mu$	$\text{LogNormal}(\log(1/8), 0.2/\sqrt{\gamma_2})$
Reporting delay (lag)	$D$	$\text{LogNormal}(\log(8), 0.2/\sqrt{\gamma_3})$
Initial number of infected individuals	$I_0$	$\text{Gamma}(2\gamma_4 - \gamma_4 + 1, 20/\gamma_4)$
Noise dispersion	$\psi$	$\text{Exponential}(5/\gamma_5)$

*Note.* Our parameterization follows the `numpy` library’s implementation of the respective distribution.

We use time-series data from the first two weeks of the COVID-19 pandemic in Germany provided by the Center for Systems Science and Engineering (CSSE) at Johns Hopkins University, licensed under CC BY 4.0.<sup>2</sup>

**Neural Network and Training:** Our neural network architecture follows a simplified version of the design implemented by Radev et al. (2021b): We use a recurrent network with gated recurrent units as summary network and a conditional invertible network as inference network.

All computations for this experiment were performed on a single-GPU machine with an NVIDIA RTX 3070 graphics card and an AMD Ryzen 5 5600X processor. Simulating 16 384 training data sets took 8 seconds and subsequent offline training 6 minutes.

**Additional Results:** We additionally train a standard neural approximator without prior context  $C_P$  to ensure that amortized prior sensitivity does not decrease approximation performance. Figure 7 and Figure 8 show similar parameter recovery, both limited by the small number of  $T = 14$  data points available. Figure 9 and Figure 10 demonstrate that calibrated

<sup>2</sup>[https://raw.githubusercontent.com/CSSEGISandData/COVID-19/master/csse\\_covid\\_19\\_data/csse\\_covid\\_19\\_time\\_series/time\\_series\\_covid19\\_confirmed\\_global.csv](https://raw.githubusercontent.com/CSSEGISandData/COVID-19/master/csse_covid_19_data/csse_covid_19_time_series/time_series_covid19_confirmed_global.csv)

predictions are nevertheless achievable, with equal patterns between SA-ABI (Figure 9) and standard ABI (Figure 10) for the baseline  $\gamma = 1.0$  setting. Figure 11 additionally contains MMD hypothesis tests that clearly show sensitivity of the parameter posterior to the prior specification.

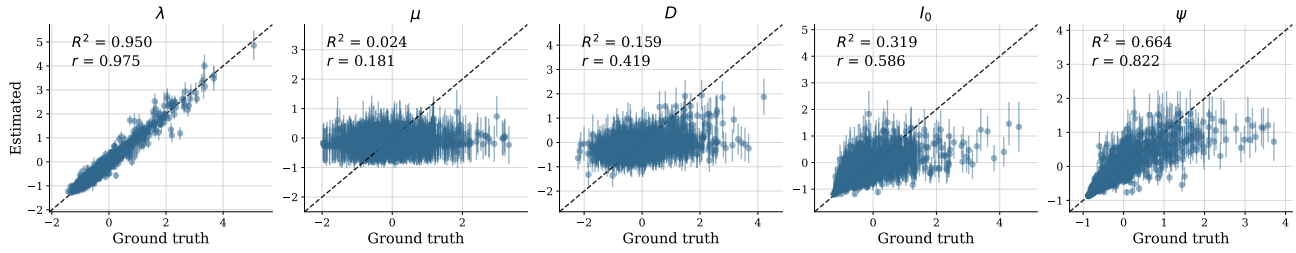


Figure 7: **Experiment 1.** Simulation-based recovery of the context-aware neural approximator used in our experiment for  $\gamma = 1.0$ .

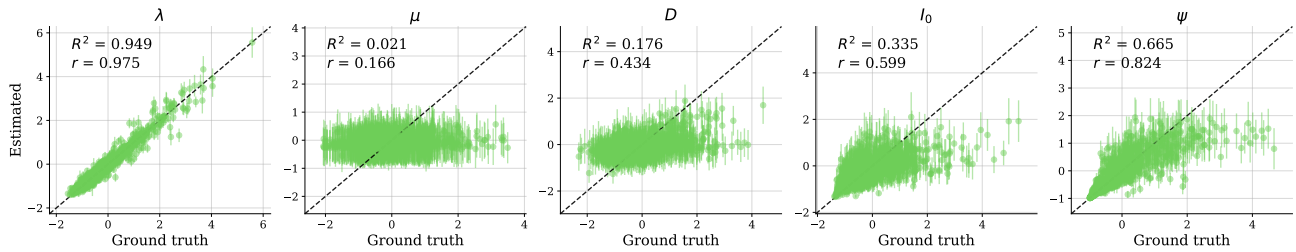


Figure 8: **Experiment 1.** Simulation-based parameter recovery of a single-prior neural approximator trained with the same configuration and budget as in our experiment but without  $C_P$  (i.e., on the baseline  $\gamma = 1.0$  setting).

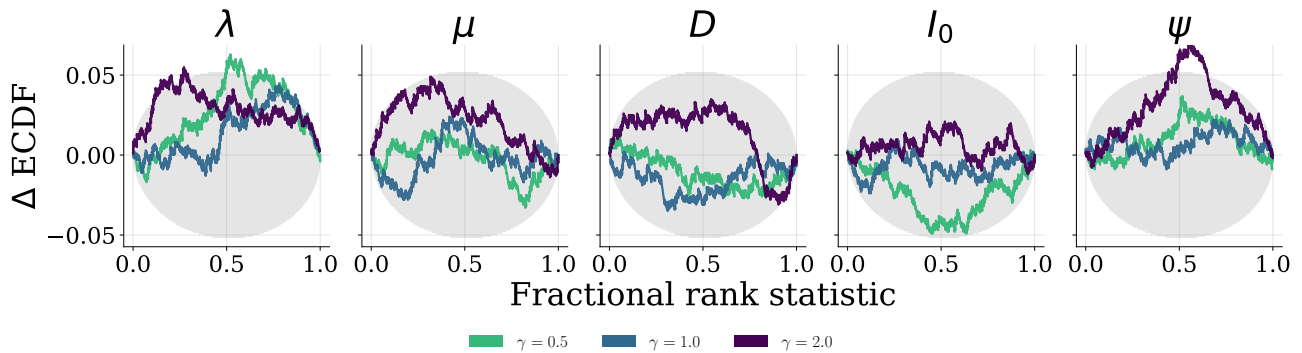


Figure 9: **Experiment 1.** Simulation-based calibration of the context-aware neural approximator used in our experiment for all three contexts  $\gamma \in \{0.5, 1.0, 2.0\}$ .

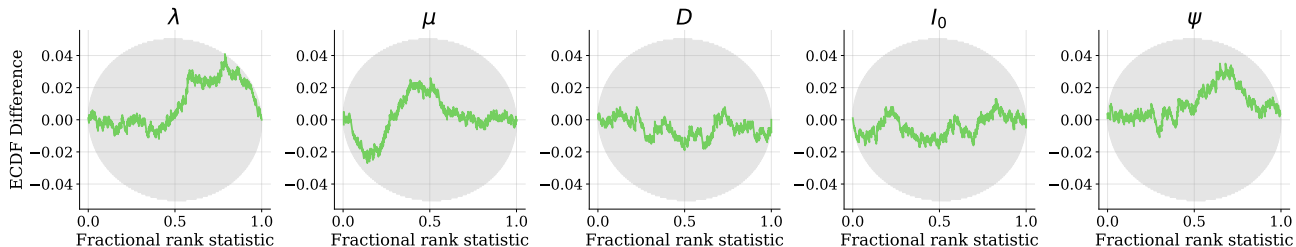


Figure 10: **Experiment 1.** Simulation-based calibration of a single-prior neural approximator trained with the same configuration and budget as in our experiment but without  $C_P$  (i.e., on the baseline  $\gamma = 1.0$  setting).

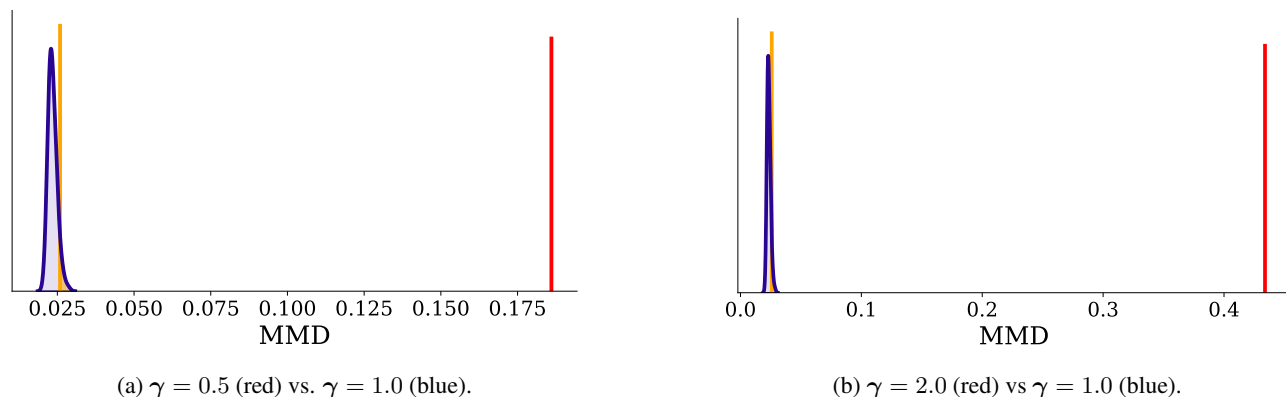


Figure 11: **Experiment 1.** MMD hypothesis tests confirm sensitivity to prior specification in the parameter space. The blue density represents samples under the null distribution of zero difference between  $\gamma = 1.0$  and the scaled posteriors (red;  $\gamma = 0.5$  or  $\gamma = 2.0$ ), the yellow lines mark the area with a  $\delta = 5\%$  rejection probability.

### C.3 Experiment 2: Climate Trajectory Forecasting

**Data:** Climate models (CM) are typically differential equations describing all relevant components of the Earth system and their couplings. Socioeconomic pathways (SSPs) provide comprehensive scenarios of future developments by describing qualitatively different trajectories of future emissions. Following standard practice, we append the associated radiative forcing in the year 2100 to the SSP identifier (e.g., SSP1-2.6 refers to the SSP1 scenario with radiative forcing of  $2.6W/m^2$ ). Given a CM, an SSP, and an initial condition (IC), high-dimensional trajectories of many observables can be simulated from the underlying model. Here we restrict the analysis to the air temperature at the surface (TAS).

Simulations produce trajectories  $TAS^{CM, SSP, IC}(\vec{x}, t)$  where  $\vec{x}$  is a spatial coordinate on the Earth’s surface and  $t$  is a time between 1850 and 2100. From this, the area-weighted global mean surface air temperature (GSAT) can be computed, which is the key indicator of global warming over pre-industrial levels.

All data used in this experiment is freely available to download: For the climate model simulation outputs, we use data from the Earth System Grid Federation.<sup>3</sup> For the observational data set for 2022, we use data from Berkeley Earth, licensed under CC BY 4.0.<sup>4</sup> We include all climate models that have archived at least 10 trajectories for the future emission scenarios SSP1, SSP2, and SSP3 in our analysis. We reshape all data to a  $2.5 \times 2.5$  longitude-latitude grid and compute yearly differences to the baseline period (1951 to 1980). The warming threshold is defined relative to the pre-industrial period 1850 to 1900, from which we can directly obtain the time-to-threshold parameter  $\theta$  for each tuple of year, model, and trajectory ensemble.

**Model Setup:** Our model setup focuses on the time  $\theta$  until the  $1.5^\circ C$  warming threshold is reached, but can easily be adapted to arbitrary temperature thresholds. We realize a prior context  $C_P$  for  $\theta$  by two discrete prior choices (see Figure 12: First, a weakly informative prior,  $\theta \sim \mathcal{U}(-40, 41)$ , that encompasses the full range of values present in the

<sup>3</sup><https://esgf.llnl.gov/>

<sup>4</sup><https://berkeleyearth.org/data/>

training data of simulated climate warming trajectories. Second, a more informative Gaussian prior,  $\mathcal{N}_+(10, 10)$ , truncated to include only positive values. This prior is based on the IPCC sixth assessment report stating that the central estimate of crossing the 1.5°C threshold lies in the early 2030s (Lee et al., 2021).

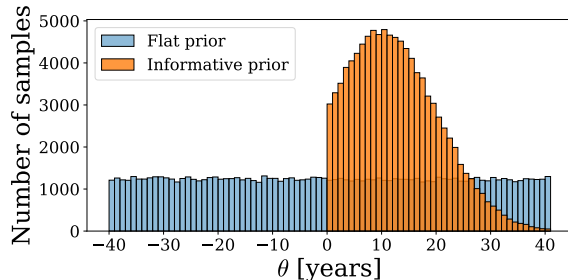


Figure 12: **Experiment 2.** Prior predictive distributions of the weakly informative (flat) prior and the informative prior constituting the prior context  $C_P$ .

Table 5: Overview of the climate models included in each SSP emission scenario.

Climate Models	SSP1-2.6	SSP2-4.5	SSP3-7.0
ACCESS-ESM1-5	✓	✓	✓
CanESM5	✓	✓	✓
CESM2			✓
CNRM-ESM2-1		✓	
GISS-E2-1-G		✓	✓
IPSL-CM6A-LR		✓	✓
MIROC-ES2L	✓	✓	✓
MIROC6	✓		
UKESM1-0-LL	✓		✓

The likelihood is obtained from the simulated trajectories of the climate models. For a given time-to-threshold  $\theta$  and climate model (encoded in the likelihood context  $C_L$ ), trajectories of the respective climate model are selected in ensembles of 10. We first identify the year of threshold exceedance of the mean global surface temperature across a trajectory ensemble.<sup>5</sup> Afterwards, a random ensemble and trajectory are chosen. Finally, the likelihood algorithm returns the spatial temperature pattern that is  $\theta$  years prior to the year of threshold exceedance in the simulated trajectory.

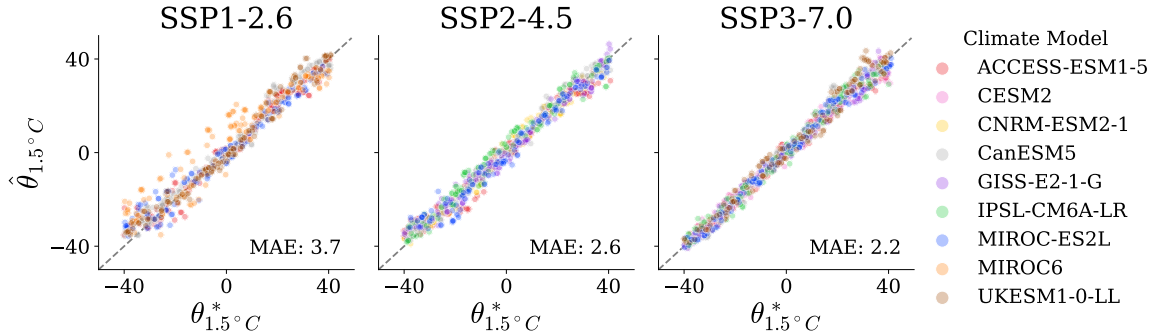
**Neural Network and Training:** We z-standardize data and parameters before passing them to the neural approximator. As summary network, we use a dense network that parallels the architecture used in Diffenbaugh and Barnes (2023): Inputs come in the form of 72x144 temperature grids and are flattened. Two hidden layers of 25 units with ReLU activation are followed by 8 output units of learned summary statistics. During training, we additionally employ dropout regularization with a dropout probability of 0.4 on the initial layer of the summary network to mitigate overfitting. As inference network, we use a conditional invertible neural network. Since normalizing flows require more than one dimension, we add a dummy standard normal parameter.

Training the neural approximator took approximately 70 minutes on a consumer notebook with a 6-core AMD Ryzen 5 5625U CPU and without a dedicated graphics card, underscoring the wide applicability of our method.

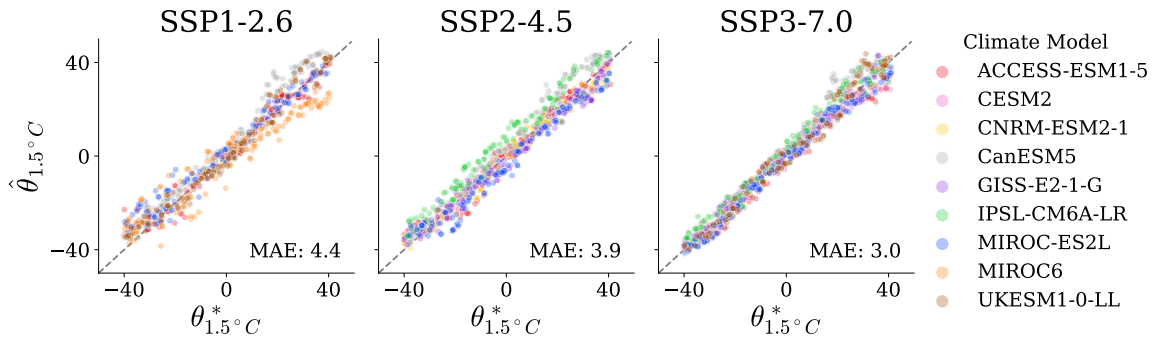
For the individual ABI instances trained for the benchmark, each instance was trained on data of a specific scenario  $\times$  climate model setting. We used the same network architecture for separate and joint training to enhance comparability, but note that the hyperparameters may not be optimal for the respective data size settings. Joint training was conducted on 80 epochs, whereas we chose a smaller number of 15 epochs for the separate training to mitigate overfitting.

<sup>5</sup>Averaging over trajectory ensembles smoothes out the chaotic internal variability to obtain a more stable estimate. In contrast, the IPCC defines the year of threshold exceedance as the middle of a 20-year averaging window. Diffenbaugh and Barnes (2023) show that resulting forecasts are insensitive to the chosen definition.

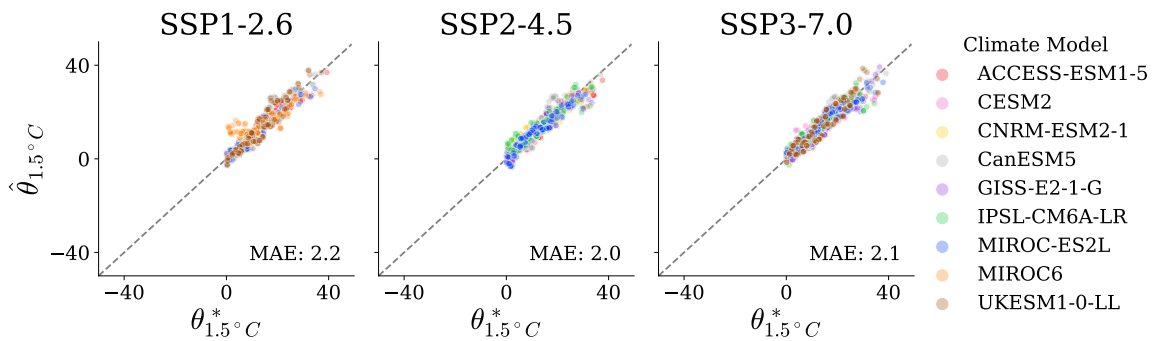
**Additional Results:** To validate our approach, we compute the mean absolute error (MAE) of the point estimate (posterior mean)  $\hat{\theta}$  to the true value  $\theta^*$  on a held-out validation set. [Figure 13a](#) shows good recovery across climate models, true time-to-threshold  $\theta^*$ , and SSPs. To parallel the evaluation procedure of Diffenbaugh and Barnes (2023), who did not differentiate between the climate models, we use a flat prior via the prior context  $C_P$  and marginalize predictions over all climate models contained in  $C_L$ . [Figure 13b](#) shows that our sensitivity-aware approach does not sacrifice predictive accuracy and further enables the identification of biased estimates for MIROC6 in the SSP1-2.6 scenario as the main limitation to better performance. [Figure 14](#) provides an additional perspective via standard simulation-based recovery and calibration plots. Overall recovery is high, but calibration plots indicate notable underconfidence of the posteriors, implying that the networks systematically overestimate the variance of time-to-threshold  $\theta$  predictions. We hypothesize that this is due to an underperforming summary network which we nevertheless keep the same as in Diffenbaugh and Barnes (2023) for the sake of comparability.



(a) Weakly informative prior. Recovery with  $C_L$  information about the respective climate model given is good (total MAE of 2.0) across climate models, true time-to-threshold  $\theta^*$ , and SSPs.



(b) Weakly informative prior. Recovery without  $C_L$  information about the respective climate model given – all predictions are not only obtained for the appropriate climate model, but all climate models contained in  $C_L$  and afterwards averaged. This leads to a validation setup comparable to Diffenbaugh and Barnes (2023). The mean absolute error (MAE) of 3.0 years for SSP3-7.0 indicates that our approach does not sacrifice predictive accuracy in comparison to Diffenbaugh and Barnes (2023), who report MAE between 2.7 and 3.8 years for the same task (eyeballed values from boxplots reported in the appendix).



(c) Informative prior. Recovery with  $C_L$  information about the respective climate model given, here restricted to positive  $\theta$  values due to the truncation of the prior. Recovery is good with a total MAE of 1.2.

Figure 13: **Experiment 2.** Recovery of time-to-threshold on held-out validation data.

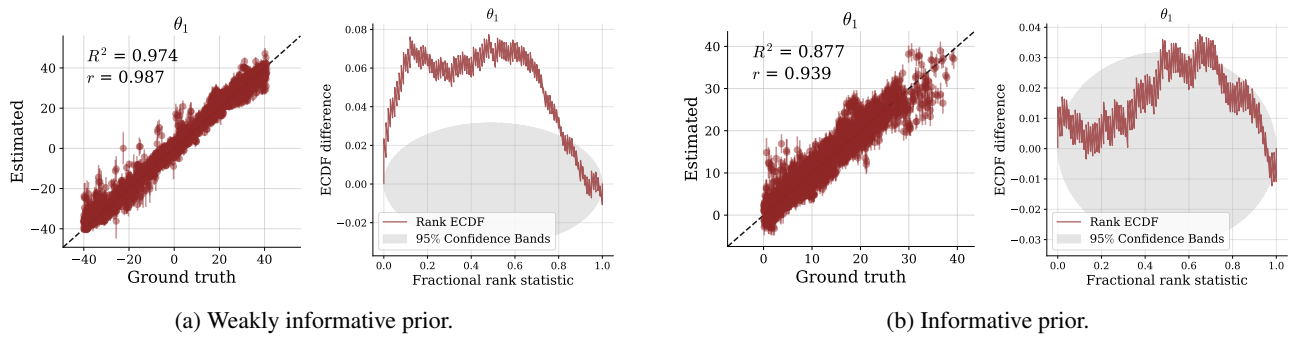


Figure 14: **Experiment 2.** Standard simulation-based metrics of recovery and calibration on held-out validation data for both prior contexts  $C_P$ . Information  $C_L$  about the respective climate model given and marginal results over climate models and SSPs are displayed.

### C.4 Experiment 3: Comparing Hierarchical Models of Decision-Making

**Model Setup:** The drift-diffusion model (DDM; Ratcliff, 1978; Ratcliff et al., 2016) models binary decision outcomes and their associated response times with the following stochastic ordinary differential equation:

$$dx = v dt + \xi \sqrt{dt} \quad (22)$$

$$\xi \sim \mathcal{N}(0, 1), \quad (23)$$

with  $dx$  denoting the change in evidence accumulation,  $v$  denoting the rate of evidence accumulation, and  $\xi$  the noise of evidence accumulation. Additional parameters of the model include the non-decision time  $t_0$  (e.g., encoding and motor response), the decision threshold  $a$ , and the bias towards a decision option  $z_r$ .

The Lévy flight model (LFM; Voss et al., 2019) relaxes the Gaussian noise assumption by using the more general  $\alpha$ -stable distribution, leading to an unknown analytical form of the likelihood:

$$dx = v dt + \sigma d\xi \quad (24)$$

$$\xi \sim \text{AlphaStable}(\alpha, \mu = 0, \sigma = \frac{1}{\sqrt{2}}, \beta = 0), \quad (25)$$

with the additional stability parameter  $\alpha$  which shall also be estimated.

Additionally, there is a debate about whether the model parameters  $v$ ,  $z_r$ , and  $t_0$  should have a fixed value over the course of an experiment (basic models) or be allowed to vary (full models) throughout the experiment (Boehm et al., 2018; Lerche & Voss, 2016). Therefore, we compare the following four models in this experiment: basic DDM ( $\mathcal{M}_1$ ), basic LFM ( $\mathcal{M}_2$ ), full DDM ( $\mathcal{M}_3$ ), and full LFM ( $\mathcal{M}_4$ ). As in Elsemüller et al. (2023), we reanalyze data by Wieschen et al. (2020) (provided by the original authors) containing 40 participants with 900 decision trials each and assume a uniform model prior (i.e., equal prior model probabilities). We use the same hierarchical priors as Elsemüller et al. (2023), who provided a detailed table with all prior choices. Since they are central to our experiment, we reiterate the priors leading to  $\alpha_m$  for each participant  $m$  here:

$$\begin{aligned} \mu_\alpha &\sim \mathcal{N}(1.65, 0.15/\gamma_1) \\ \sigma_\alpha &\sim \mathcal{N}_+(0.3, 0.1/\gamma_2) \\ \alpha_m &\sim \mathcal{N}_{Truncated}(\mu_\alpha, \sigma_\alpha, 1, 2) \text{ for } m = 1, \dots, M. \end{aligned} \quad (26)$$

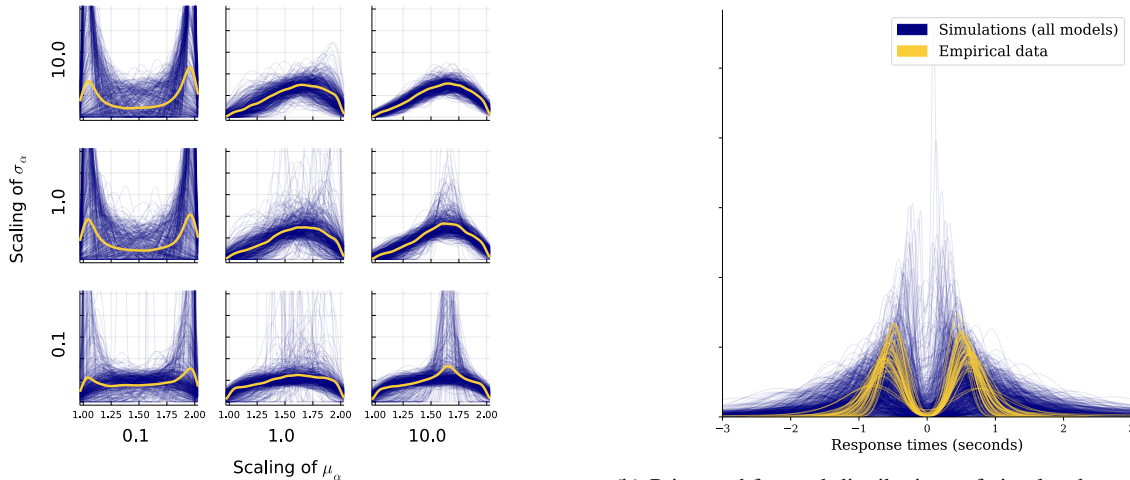
Our experiment investigates the sensitivity to different  $C_P$ ,  $C_A$ , and  $C_D$  realizations. For  $C_P$ , we power-scale the hierarchical prior of  $\alpha$  with a wide range of  $\gamma \in [0.1, 10]$ , which would have been infeasible with existing methods since they require values close to the mid-range value of no scaling, i.e.,  $\gamma = 1$  (Kallioinen et al., 2021). To ensure equal amounts of widening and shrinking of the respective distributions during training, we draw the scaling factors from independent uniform distributions in the log space  $\gamma \sim \exp(\mathcal{U}(\log(0.1), \log(10)))$ . Figure 15a displays the prior predictive distribution of  $\alpha$  under different  $\gamma$  configurations. We use 100 bootstrap samples on the trial level (i.e., within the observations of each participant) for the data context  $C_D$  and describe the details of the approximator context  $C_A$  in the following section.

**Neural Network and Training:** All 20 members of the employed deep ensemble constituting  $C_A$  are set up and trained independently and identically. Each network uses a hierarchical summary network consisting of two permutation invariant deep set networks (Zaheer et al., 2017) and a standard feedforward network with a softmax output layer as an inference network.

As in Elsemüller et al. (2023), we first pre-train each network on smaller data sets of 40 simulated participants with 100 observations each, and afterwards fine-tune on the full data size of 40 simulated participants with 900 observations. We use 30 epochs for both phases and an Adam optimizer (Kingma & Ba, 2015) with a cosine decay schedule (initial learning rates of  $5 \times 10^{-4}$  for pre-training and  $5 \times 10^{-5}$  for fine-tuning).

All computations for this experiment were performed on a single-GPU machine with an NVIDIA RTX 3070 graphics card and an AMD Ryzen 5 5600X processor. Simulating 40 000 pre-training and 8 000 fine-tuning data sets in the Julia programming language (Bezanson et al., 2017) took 23 minutes. Training the deep ensemble took 21 minutes for pre-training and 45 minutes for fine-tuning per network.

**Additional Results:** Figure 15b displays the prior pushforward distribution of simulated response times and the empirical response times. The informative priors from Elsemüller et al. (2023) assign high densities to the central regions of the



(a) Prior predictive distributions of the  $\alpha$  parameter under power-scaling. The yellow line represents the marginal density for each configuration.

(b) Prior pushforward distributions of simulated response times per person contrasted with the empirical distributions per person. Negative response times indicate a decision for the lower decision boundary and positive times for the upper decision boundary.

Figure 15: **Experiment 3.** Prior distributions. **a)** Prior predictive distributions of the  $\alpha$  parameter under maximum widening ( $\gamma = 0.1$ ), no scaling ( $\gamma = 1$ ), and maximum shrinkage ( $\gamma = 10$ ) of the hyperpriors  $\mu_\alpha$  and  $\sigma_\alpha$ . **(b)** Prior pushforward distributions of the response times simulated by the four compared models (marginalized over  $\gamma$ ) and the empirical response times.

empirical distribution. Nevertheless, the results of the typical set approach (Morningstar et al., 2021; Nalisnick et al., 2019) in Figure 16 flag the empirical data as out-of-distribution of the deep ensemble.

To ensure that the inclusion of  $C_P$  in the amortization scope does not lead to a substantially worsened approximation performance, we trained an additional deep ensemble without  $C_P$ . Table 6 displays validation performance and empirical approximations for the ensemble including  $C_P$  and Table 7 for the ensemble without  $C_P$ . Including  $C_P$  does neither lead to a substantial drop in performance nor qualitatively different model comparison results despite power-scaling over a wide range.

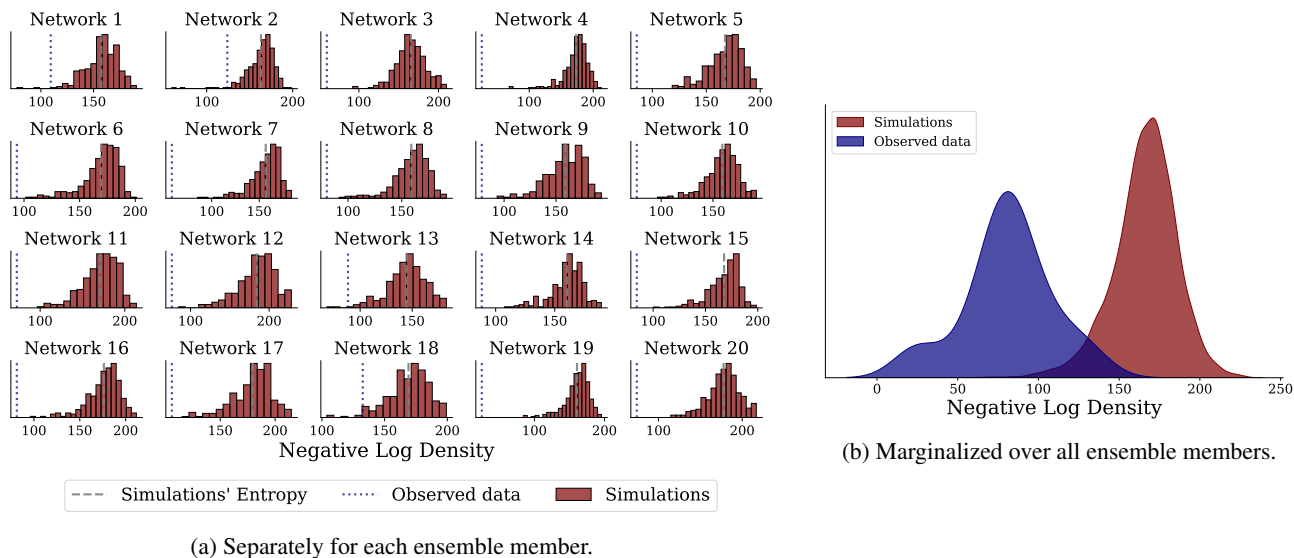


Figure 16: **Experiment 3.** The typical set of summary statistics from the model simulations (considering  $C_P$  and  $C_A$ ) contrasted with the density of the summary statistics from the observed data. Both a) separate and b) joint assessment flags the empirical data as out-of-distribution.

Table 6: **Experiment 3.** Validation performance on 8 000 held-out simulations and predictions on the empirical data of the deep ensemble trained on power-scaled  $C_P$  context from 0.1 to 10.

	Validation Performance				Empirical Predictions			
	ECE	Brier Score	MAE	Accuracy	$\mathcal{M}_1$	$\mathcal{M}_2$	$\mathcal{M}_3$	$\mathcal{M}_4$
Network 1	0.01	0.01	0.02	0.99	0.00	0.00	1.00	0.00
Network 2	0.01	0.03	0.05	0.96	0.00	0.00	0.92	0.08
Network 3	0.01	0.01	0.01	0.99	0.00	0.00	0.17	0.83
Network 4	0.01	0.01	0.01	0.99	0.00	0.00	0.50	0.50
Network 5	0.01	0.01	0.01	0.99	0.00	0.00	0.96	0.04
Network 6	0.01	0.01	0.01	0.99	0.00	0.00	0.02	0.98
Network 7	0.01	0.01	0.01	0.99	0.00	0.00	0.75	0.25
Network 8	0.01	0.01	0.02	0.99	0.00	0.00	1.00	0.00
Network 9	0.01	0.01	0.01	0.99	0.52	0.03	0.25	0.21
Network 10	0.01	0.02	0.03	0.97	0.00	0.00	0.85	0.15
Network 11	0.01	0.01	0.01	0.99	0.00	0.00	0.37	0.63
Network 12	0.01	0.01	0.01	0.99	0.00	0.00	0.00	1.00
Network 13	0.01	0.01	0.01	0.99	0.00	0.00	0.99	0.01
Network 14	0.01	0.02	0.03	0.98	0.00	0.00	0.99	0.01
Network 15	0.01	0.01	0.01	0.99	0.00	0.96	0.00	0.04
Network 16	0.00	0.00	0.01	0.99	0.97	0.00	0.03	0.00
Network 17	0.01	0.02	0.02	0.98	0.00	0.00	0.62	0.38
Network 18	0.01	0.02	0.03	0.98	0.00	0.00	0.91	0.09
Network 19	0.01	0.01	0.01	0.99	0.00	0.04	0.49	0.46
Network 20	0.01	0.01	0.01	0.99	0.00	0.00	0.08	0.92
Average	0.01	0.01	0.02	0.99	0.07	0.05	0.54	0.33
Std. Deviation	0.00	0.01	0.01	0.01	0.24	0.21	0.40	0.36

Table 7: **Experiment 3.** Validation performance on 8 000 held-out simulations and predictions on the empirical data of the deep ensemble trained without  $C_P$  context.

	Validation Performance				Empirical Predictions			
	ECE	Brier Score	MAE	Accuracy	$\mathcal{M}_1$	$\mathcal{M}_2$	$\mathcal{M}_3$	$\mathcal{M}_4$
Network 1	0.00	0.00	0.00	1.00	0.00	0.00	0.01	0.99
Network 2	0.00	0.01	0.01	0.99	0.00	0.00	0.00	1.00
Network 3	0.01	0.01	0.02	0.98	0.00	0.00	0.99	0.01
Network 4	0.01	0.02	0.03	0.98	0.00	0.00	0.60	0.40
Network 5	0.01	0.01	0.03	0.98	0.00	0.00	0.88	0.12
Network 6	0.00	0.00	0.00	1.00	1.00	0.00	0.00	0.00
Network 7	0.00	0.00	0.00	1.00	0.00	0.00	0.00	1.00
Network 8	0.01	0.01	0.02	0.98	0.00	0.00	0.00	1.00
Network 9	0.00	0.00	0.00	1.00	0.00	1.00	0.00	0.00
Network 10	0.00	0.00	0.00	1.00	0.72	0.16	0.11	0.00
Network 11	0.00	0.00	0.00	1.00	0.01	0.42	0.00	0.56
Network 12	0.01	0.02	0.04	0.97	0.00	0.00	0.91	0.09
Network 13	0.01	0.01	0.01	0.99	0.00	0.00	0.00	1.00
Network 14	0.00	0.00	0.00	1.00	0.00	0.00	1.00	0.00
Network 15	0.01	0.01	0.01	0.99	0.00	0.00	1.00	0.00
Network 16	0.00	0.00	0.00	1.00	0.00	0.00	0.98	0.02
Network 17	0.00	0.00	0.00	1.00	0.00	0.25	0.01	0.74
Network 18	0.00	0.00	0.00	1.00	0.00	0.00	0.86	0.14
Network 19	0.01	0.01	0.01	0.99	0.00	0.00	0.00	1.00
Network 20	0.01	0.02	0.04	0.97	0.00	0.00	0.88	0.11
Average	0.00	0.01	0.01	0.99	0.09	0.09	0.41	0.41
Std. Deviation	0.01	0.01	0.01	0.01	0.27	0.24	0.46	0.44